Reprints

RSC Advances

PAPER

View Article Online
View Journal | View Issue

Cite this: *RSC Adv.*, 2014, **4**, 49819

Electrochemical detection of adenine and guanine using a self-assembled copper(II)–thiophenyl-azo-imidazole complex monolayer modified gold electrode†

Koushik Barman and Sk Jasimuddin*

Received 13th August 2014
Accepted 29th September 2014

DOI: 10.1039/c4ra08568j

www.rsc.org/advances

Electrochemical detection of adenine (A) and guanine (G) using the self-assembled monolayer of copper(II)–thiophenyl-azo-imidazole modified gold electrode (Cu^{2+}–IATP–Au) is reported. The self-assembled momolayer of 4-(2′-imidazolylazo)thiophenol (IATP) on a gold electrode surface was prepared by covalent immobilization of imidazole onto a 4-aminothiophenol monolayer modified gold electrode by a diazotization-coupling reaction. The catalyst was formed by immobilizing Cu(II) ion on the IATP modified gold electrode. The modified gold electrode was characterised by Field emission scanning electron microscopy, Energy dispersive X-ray analysis, Infrared spectroscopy, Cyclic voltammetry and Electrochemical Impedance spectroscopic techniques. The Cu^{2+}–IATP–Au electrode exhibits excellent electrocatalytic activity towards the oxidation of A and G. Without separation or pre-treatment, the modified electrode can detect A and G simultaneously in a mixture and DNA samples. In the presence of excess common interferents such as ascorbic acid, citric acid, cysteine, glucose, Na^+, K^+, Cl^-, SO_4^{2-} had no effect on the peak current of A and G. In differential pulse voltammetry measurement, the oxidation current response of A and G was increased linearly in the concentration range 10–60 μM and the detection limit was found to be 0.06 μM and 0.01 μM ($S/N = 3$), respectively. The proposed method was applied to determine adenine and guanine in herring sperm DNA and the result was satisfactory.

1. Introduction

Adenine (A) and Guanine (G) are the building blocks of nucleic acids and play an important role in genetic information storage and protein biosynthesis and fulfill a variety of functions in the metabolism of the cell.[1] The abnormal changes of the concentration of A and G in nucleic acid may cause several diseases, including Parkinson's disease, carcinoma and liver diseases.[2] Hence, the determination of A and G has great significance in bioscience and clinical diagnosis. Various methods have been applied for their detection and measurement, such as chromatography,[3] electrophoresis,[4] chemical luminescence,[5] spectrophotometry[6] or surface enhanced Raman scattering.[7] These methods are excellent but have several shortcomings such as high cost, high time consumption and tedious pretreatment steps.

For routine analysis electrochemical techniques are very promising due to low cost, high sensitivity, high selectivity and ease of miniaturization. They are suitable for analysis of A and G individually or simultaneously,[8] still the electrochemical methods suffer problems for the detection of nucleic bases such as slow electron transfer kinetics, high overpotential and overlapping of their oxidation peaks. To overcome the problems, chemical modification of electrode surface with suitable materials is always beneficial. Varieties of materials have been used for the electrode surface modification and used them to electrochemical detection of A and G. Cyclodextrin modified poly(*N*-acetylaniline) film,[9] Graphene oxide intercalated by self-doped polyaniline nanofibers[10] or cobalt(II)phthalocyanine modified carbon paste electrode,[11] Porous silicon supported Pt–Pd nanoalloy modified carbon nanotube paste electrode,[12] glassy carbon electrode modified with overoxidized polypyrrole/graphene,[13] multiwall carbon nanotubes (MWCNTs) decorated with $NiFe_2O_4$ magnetic nanoparticles,[14] silver nanoparticles(AgNPs)–polydopamine(Pdop)@graphene(Gr)composite,[15] single-stranded DNA–poly(sulfosalicylic acid)composite film,[16] TiO_2 nanobelts,[17] graphene-COOH,[18] 1,8,15,22-tetraaminophthalocyanatonickel(II),[19] Iron hexacyanoferrate film,[20] azocalixarene,[21] graphene–Nafion composite film,[22] fullerene-C_{60} (ref. 23) and gold electrode modified with *n*-octadecylmercaptan, followed by controllable adsorption of graphene sheets[24] have been used for the electrochemical oxidation and detection of A and G. However, these modified electrodes have some drawbacks such as stability,

Department of Chemistry, Assam University, Silchar, Assam-788011, India. E-mail: j.seikh@gmail.com; Fax: +91-0342-270802; Tel: +91-0342-270848

† Electronic supplementary information (ESI) available: Cyclic voltammogram, differential pulse voltammogram. See DOI: 10.1039/c4ra08568j

reproducibility and use of costly chemicals for electrode modification. In this context, the development of novel, chip and simple strategy for electrode modification is highly desirable. Diazonium salt has been extensively used for the electrode surface modification.[25] Diazonium group functionalized electrode surface can coupled with phenolic, imidazole or amino groups to form different diazotized compounds[26] which are capable of forming metal complexes. There are many reports that metal-azo complexes can interact with the DNA bases and is important in the field of anticancer drug research.[27] A and G formed complexes with metals including copper, has been extensively studied by electrochemical methods.[28] A number of articles have been devoted to the catalytic and electrocatalytic activity of copper(II) modified electrode for the redox reaction of organic and biological compounds. For example, electrocatalytic oxidation of hydroquinone with copper(II)-L-cysteine[29] and copper(II)-5-amino-2-mercaptobenzimidazole[30] complex monolayer modified gold electrode, catalytic oxidation of L-cysteine in oxygen-saturated aqueous solution by copper(II) supported on a polymer,[31] determination of cysteine at a glassy carbon electrode modified by copper(II) ions,[32] determination of ascorbic acid using dinuclear copper salicylaldehyde-glycine schiff base modified GC electrode[33] and copper(II)–zeolite modified electrode,[34] electrocatalytic oxidation of carbohydrates at copper(II) oxide modified electrode[35] and certain catecholamines such as dopamine, L-dopa, epinephrine and norepinephrine using copper(II) complex and AgNPs modified glassy carbon paste electrode.[36]

In the present study, we have used a self assembled copper(II) containing azoimidazole complex modified gold electrode for the detection of purine bases, A and G, individually and simultaneously in the physiological pH. Electrode modification process and the electrochemical oxidation behaviour of A and G over the modified electrode were studied in detail. The modified electrode has also been applied for the detection of DNA bases in real sample.

2. Experimental

2.1. Chemicals and reagents

4-Aminothiophenol (4-ATP) and $NaClO_4$ were purchased from Sigma-Aldrich (India). Imidazole, $CuSO_4 \cdot 5H_2O$, and $K_4[Fe(CN)_6] \cdot 3H_2O$ were purchased from Merck (India) and were used as received. Denatured herring sperm DNA, A, G were purchased from Sigma-Aldrich (India). Phosphate buffer solution was prepared by mixing 0.1 M $NaClO_4$ and 0.01 M H_3PO_4 and the pH's were adjusted by the addition of 0.11 M NaOH using Smalley's method.[37] Water was purified by double distillation with alkaline $KMnO_4$.

2.2. Apparatus and instrumentations

The field emission scanning electron microscopy (FE SEM) images and Energy dispersive X-ray (EDAX) analysis data were obtained using FE-SEM, FEI INSPECT F50 operated at an acceleration voltage of 20 kV. FTIR spectra were recorded on a Shimadzu 8400S spectrometer. Electrochemical measurements were performed on a CHI 660C Electrochemical workstation (CH Instrument, USA). A three electrode system was employed with gold or modified gold electrode as working electrode, Pt wire as counter electrode and Ag/AgCl (3 M KCl) as reference electrode. The pH measurements of solutions were carried out on a pH meter (Macro Scientific works (Regd), New Delhi).

2.3. Electrode pre-treatment and immobilization of 4-(2′-imidazolylazo)thiophenol over gold electrode

A gold electrode (2 mm in diameter) was polished with 0.05 μm α-alumina on a polishing pad and rinsed extensively with anhydrous ethanol and distilled water. Then the gold electrode was electrochemically cleaned in 0.5 M H_2SO_4 until a steady characteristic gold oxide cyclic voltammogram was obtained.[38] The cleaned gold electrode was immersed into the 4-ATP (1 mM) solution for 20 hours. The self-assembled 4-ATP monolayer was formed over electrode surface *via* gold–sulfur interaction and the modified electrode was thoroughly washed with ethanol and distilled water. After that the 4-ATP–Au electrode was dipped into a 0.1 M HCl solution at 2–4 °C, and 0.1 g $NaNO_2$ solution was added slowly. After 30 minute incubation, the diazotized modified gold electrode (diazo-ATP–Au) was removed and rinsed with ice cold distilled water. For coupling with imidazole, the diazo-ATP–Au electrode was immersed into aqueous 0.025 M imidazole solution for 30 minutes at 2–4 °C in stirring condition. Finally, the 4-(2′-imidazolylazo)thiophenol modified gold electrode (IATP–Au) was rinsed with distilled water and dried in air (Fig. 1).

2.4. Copper complexation on IATP–Au electrode

The IATP–Au electrode was immersed into 1×10^{-3} M $CuSO_4$ solution (containing 0.1 M KNO_3) at pH 5.6 and stirred for 4 hours. After complexation, the electrode (Cu^{2+}–IATP–Au) was washed thoroughly with distilled water and then dried in air for further experiment.

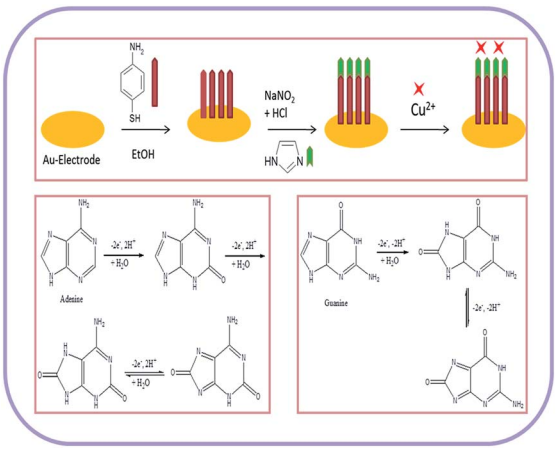

Fig. 1 Schematic representation for the fabrication of gold electrode and the electrochemical oxidation mechanism of adenine and guanine.

3. Results and discussion

3.1. Choice of materials

Copper has unique coordination chemistry which renders it suitable for many enzymatic reactions, such as superoxide dismutase (SOD), ascorbic acid oxidase, cytochrome-c-oxidase actions.[39] Imidazole moiety can be found in almost all copper(II) enzymes. In biological system, superoxide dismutase catalyses the dismutation of poisonous superoxide to O_2 and H_2O_2. Copper(II) is the catalytic center in SOD, on reduction by superoxide O_2^-, blue $[Cu^{II}(his^-)\ (his\text{-}H)_3]$ changes to colourless $[Cu^{I}(his\text{-}H)_4]$. Ascorbic acid oxidase is a blue copper(II) containing protein that catalyses the oxidation of ascorbic acid to dehydroascorbic acid by O_2. Cytochrome-c-oxidase is a terminal enzyme in the respiratory chain. It brings about the oxidation of the reduced form of $[Fe^{II}(Cyt\text{-}c)red]$ with concomitant reduction of molecular oxygen to water. These inspire us to make the biomimetic catalyst containing Cu(II)-imidazole moiety which can oxidise the purine bases, adenine and guanine and at the same time determine the concentration. Verities of nanomaterials, nano composites and few metal complexes have been used so far for electrode modification and applied for elctrocatalytic oxidation of adenine and guanine.[9–24] Similarly, different copper(II) ion modified electrodes have been used for electrocatalytic oxidation of various organic and biologically important molecules.[29–36] For the first time, we have modified gold electrode by the self-assembled copper(II)–thiophenyl-azo-imidazole complex monolayer and utilized this bio-mimetic sensor for the electrocatalytic oxidation of adenine and guanine in physiological pH. The proposed sensor exhibited a simple, rapid and sensitive determination of adenine and guanine individually as well as simultaneously with low detection limit.

3.2. Surface morphology of the Cu^{2+}–IATPmodified gold electrode

The step wise modification and surface morphology of the bare and self-assembled monolayer modified gold electrodes were characterised by FE SEM. Fig. 2(A–D) shows the clear change of surface morphology and suggested the formation of Cu^{2+}–IATP film on gold surface. EDAX images (Fig. 3(A–D)) also confirms the step wise modification. In the FTIR spectra, 4-ATP modified gold electrode shows two absorbance peaks at 3443 and 3342 cm^{-1} due to presence of NH_2 group. After diazotization and coupling with imidazole these peaks are absent but a new peak appeared at around 1376 cm^{-1} due to –N=N–bond formation. After complexation with copper(II) ion the –N=N–stretching frequency decreased due to back donation from copper to –N=N–π^* orbital and the azo peak observed at 1366 cm^{-1}. Along with these a new peak observed at 460 cm^{-1} and is due to Cu–N bond stretching which also supports the Cu^{2+}–IATP–Au modification (Fig. 4).

3.3. Electrochemical characterisation of the Cu^{2+}–IATP modified gold electrode

The stepwise modification was examined by CV using $[Fe(CN)_6]^{3-/4-}$ as redox probe in 0.1 M PBS buffer at pH 7

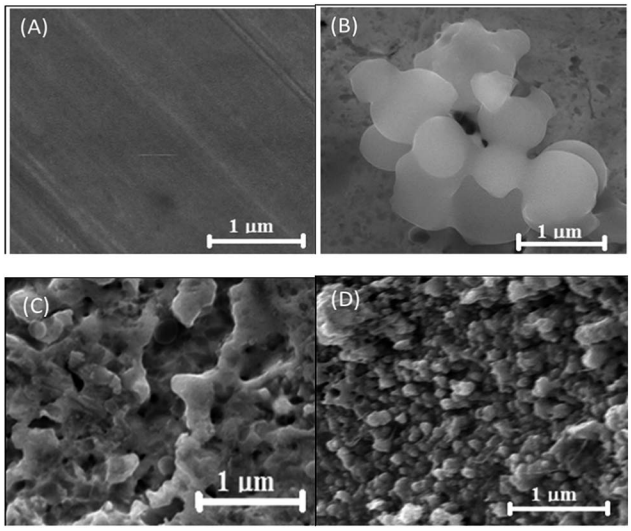

Fig. 2 SEM images of bare (A), 4-ATP modified (B), IATP modified (C), Cu^{2+}–IATP modified gold electrode (D).

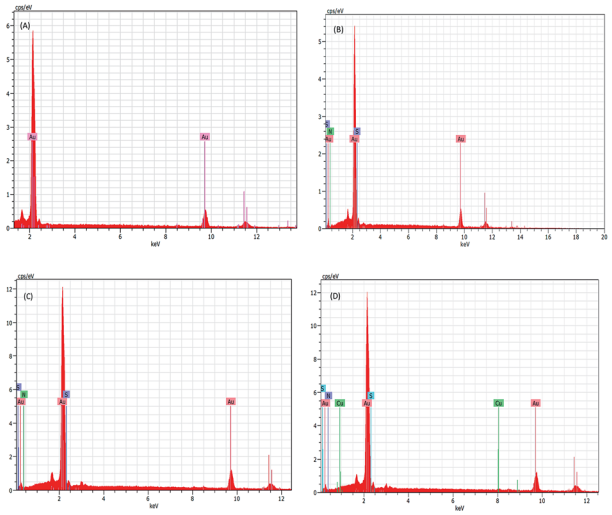

Fig. 3 EDAX spectrum of bare (A), 4-ATP modified (B), IATP modified (C), Cu^{2+}–IATP modified gold electrode (D).

(Fig. 5). For the bare electrode the cyclic voltammogram of 0.5 mM $[Fe(CN)_6]^{4-}$ exhibit electrochemically reversible redox couple. However, 4-ATP modified Au electrode, the cyclic voltammogram of $[Fe(CN)_6]^{4-}$ exhibit an irreversible feature with low current height than that of bare gold. The current height decreases even more when diazotized (diazo-ATP–Au) and imidazole coupled (IATP–Au) gold electrode was used. The experimental results indicate that the electronic communication between Au and $[Fe(CN)_6]^{4-}$ is blocked due to SAM formation. Electrochemical impedance spectroscopy supports the CV results. In the Nyquist plot the diameter of the semicircle decreases gradually when step wise modification on the gold electrode surface was carried out. The observed trend (Fig. 6) is due to the fact that the modified electrode blocked the electron transfer rate for the oxidation of $[Fe(CN)_6]^{4-}$.

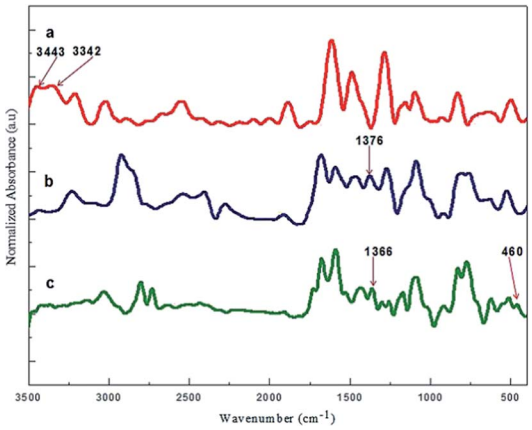

Fig. 4 FTIR spectra of (a) 4-ATP modified, (b) IATP modified and (c) Cu^{2+}–IATP modified gold electrode.

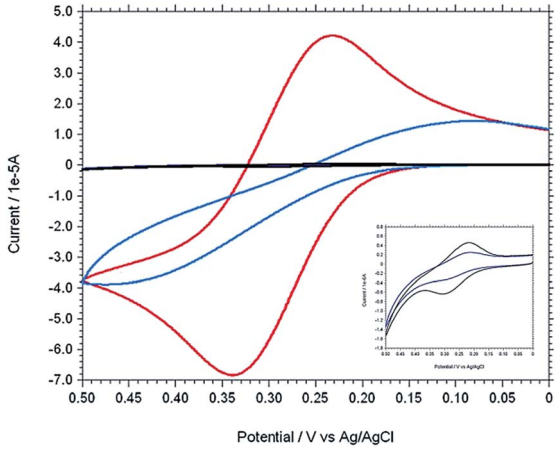

Fig. 5 Cyclic voltammograms of 0.5 mM $K_4[Fe(CN)_6]$ in 0.1 M PBS at pH 7 using different working electrode [bare Au (red), ATP–Au (light blue), ATP–N^{+2}–Au (dark blue) and IATP–Au (black)]. [Inset: enlarge figure of two overlapping curve for ATP–N^{+2}–Au (dark blue) and IATP–Au (black)].

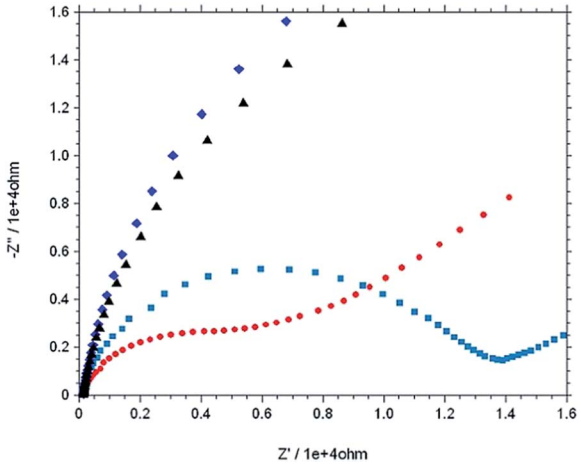

Fig. 6 Nyquist plot ($-Z''$ *versus* Z') of 0.5 mM $K_4[Fe(CN)_6]$ in 0.1 M PBS at pH = 7.0 using various working electrode from impedance measurement [bare Au (red), mod Au with 4-ATP (light blue), Au–ATP–N^{+2} (dark blue) and Au–IAT (black)], E_{ac} = 5 mv, and frequency range: 0.1 Hz to 10 000 Hz.

The IATP–Au can form a neutral monolayer at pH 7. The faradic currents for the probe redox reaction were decrease (Fig. 5) when modified the gold electrode surface with IATP. Reasonably, hydrogen bonds have more chance to form between imidazolic NH and π–π staking are more effectively formed in this condition. A value may be obtained for surface coverage $\theta = 0.99$ using $\theta = [1 - (i_p/i_p^0)]$ relation[40] where i_p^0 and i_p are peak currents of redox probe at bare and IATP–Au electrodes, respectively under the same condition. The value obtained for i_p^0 and i_p were 3.717×10^{-5} μA and 4.610×10^{-7} μA at pH = 7.0. From EIS spectra the R_{ct} was increased from bare Au (7.736×10^3 Ω) to IATP–Au (5.817×10^4 Ω). This difference is due to insulation effects originated from assemblies of neutrally charged IATP layer at pH 7. Assuming that all the current passes through pin-holes and defects, a value may be obtained for θ using $\theta = [1 - (R_{ct}^0/R_{ct})]$ relation,[40] where R_{ct}^0 and R_{ct} are the charge transfer resistance of redox probe at bare Au and IATP–Au electrodes under the similar conditions and a value of 0.87 was estimated for θ. The difference observed between θ values obtained from CV and EIS method may be attributed to the contribution of tunnelling effects.[41]

In order to confirm the Cu(II) complexation with azoimidazole on the gold surface (IATP–Au), a comparable CV was taken for bare Au, IATP–Au and Cu^{2+}–IATP–Au in 0.1 M PBS buffer at pH 7 (Fig. S1†). A Cu^{2+}/Cu^{+} redox couple ($E_{1/2} = 0.3$ V, $\Delta E = 120$ mV) supports the formation of Cu^{2+}–IATP–Au SAM. Fig. S2† shows the cyclic voltammograms for different concentration (0.1 mM to 0.7 mM) of Cu(II) ion on the IATP–Au modified electrode. Both cathodic and anodic peak current increased with increasing concentration of Cu(II) ions. The influence of pH of the electrolytic solution on the electrochemistry of Cu(II) azo-imidazole complex over Au electrode was studied. The cathodic peak current reached the maximum value at pH 7.0 (Fig. S3†) which indicates that at this pH strong complexation takes place. Electrochemical impedance spectra of the bare and modified electrodes were taken in 0.1 M PBS buffer at pH 7 and from the Nyquist plot it is clearly shows that the R_{CT} value for Cu^{2+}–IATP–Au electrode is less than IATP–Au or bare Au.

3.4. Electrochemical oxidation of adenine and guanine

The modified gold electrode Cu^{2+}–IATP–Au was used for the electrochemical oxidation of nucleobases A and G. Fig. 7 shows the cyclic voltammograms of 1 mM guanine in 0.1 M PBS (pH 7) using the bare Au (red curve), IATP–Au (blue curve) and Cu^{2+}–IATP–Au (green curve) electrodes. For bare Au and IATP–Au electrode manifested only a featureless voltammetric profile between 0 to +1.0 V whereas in case of Cu^{2+}–IATP–Au electrode two irreversible oxidation peaks appeared at +0.85 V and 0.96 V for guanine. An irreversible oxidation peak was observed at +1.2 V for adenine when Cu^{2+}–IATP–Au electrode used as working electrode (Fig. 8). No such prominent peak was observed when bare Au (red curve) and IATP–Au (blue curve) electrodes was used under similar condition. The detailed oxidation

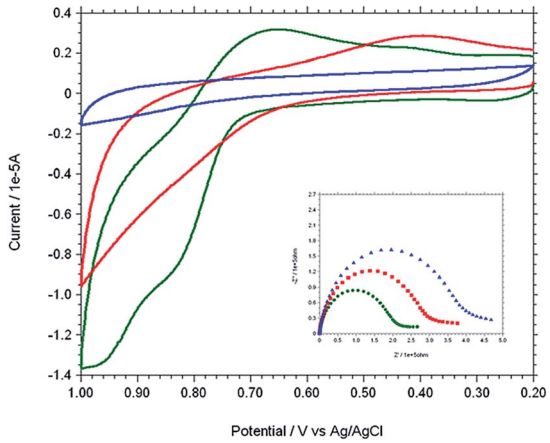

Fig. 7 Overlaid cyclic voltammogram and Nyquist plot (inset) of 1 mM Guanine in 0.1 M PBS solution at pH 7 using different working electrodes. [Bare Au (red), IATP–Au (blue) and Cu^{2+}–IATP–Au (green)].

mechanism of purine bases is shown in Fig. 1. Electrochemical oxidation of guanine followed a two step mechanism with loss of two electrons and two protons in each step and the first step was rate-determining step[42] on the other hand adenine underwent a multistep six electron six protons oxidation involving irreversible chemical steps.[43]

EIS was carried out for both A and G at pH 7.0 (PBS buffer) using the modified and bare electrodes. The diameter of the semicircle observed in the Nyquist plot corresponds to charge transfer resistance, R_{ct}; the smaller the semi-circle, faster is the charge transfer.[44] Fig. 7 and 8 (inset) shows that the diameter of semi-circle (R_{ct}) changes upon modification of gold electrode surface. The R_{ct} values in different electrode system shows the following tread: IATP–Au (3.9×10^5 Ω) > bare Au (2.9×10^5 Ω) > Cu^{2+}–IATP–Au (1.9×10^5 Ω) and IATP–Au (13.3×10^3 Ω) > bare Au (11.7×10^3 Ω) > Cu^{2+}–IATP–Au (7.2×10^3 Ω) for G and A, respectively. The observed trend is due to the fact that the copper(II) complex modified electrode ease the electron transfer rate for the oxidation of A and G whereas IATP modified gold electrode blocked the electron transfer. Electrochemical impedance measurements clearly indicate that Cu^{2+}–IATP–Au SAM modified electrode has lower resistance as compared to the bare Au and IATP–Au electrodes. This study reveals that the Cu^{2+}–IATP–Au SAM modified electrode is an efficient electrocatalyst for A and G oxidation.

3.5. Determination of adenine and guanine using DPV

Based on the optimum conditions, the individual and simultaneous determination of A and G were performed using DPV. Fig. S4† shows the DPV curves of G with different concentration. In the individual determination of purine bases the oxidation peak current of G was linear with its concentration in the range of 150–600 μM (Inset Fig. S4†). The detection limit for G is estimated to be 0.007 μM ($S/N = 3$). Fig. S5† indicated that oxidation peak current of A increased linearly in the range of 150–600 μM. The detection limit for A was 0.058 μM ($S/N = 3$). Fig. 9 shows the DPV curves of G with different concentrations in the presence of 100 μM A and the oxidation peak current of G was linear with its concentration range of 10–60 μM. The regression equation was $I_{pa} = 0.0055c + 1.3113$ ($R^2 = 0.9917$, 95% confidence limit for the slope = ±0.10 and intercept = ±0.42) with a detection limit of 0.01 μM ($S/N = 3$). Similarly, Fig. 10 shows the DPV curves of A with different concentrations in the presence of 100 μM G and the oxidation peak current of A increased linearly in the concentration range of 10–60 μM. The regression equation was $I_{pa} = 0.0088c + 2.1627$ ($R^2 = 0.9974$, 95% confidence limit for the slope = ±0.09 and intercept = ±0.31) with a detection limit of 0.06 μM ($S/N = 3$). For further evaluating the feasibility of the Cu^{2+}–IATP–Au electrode for A and G determination simultaneously by simultaneous changing their concentration (Fig. S6†). All the results indicated that the simultaneous and sensitive detection of A and G could be achieved at copper(II) complex modified gold electrode. Table 1 shows a comparison of the proposed electrochemical method and the other modified electrodes reported for adenine and

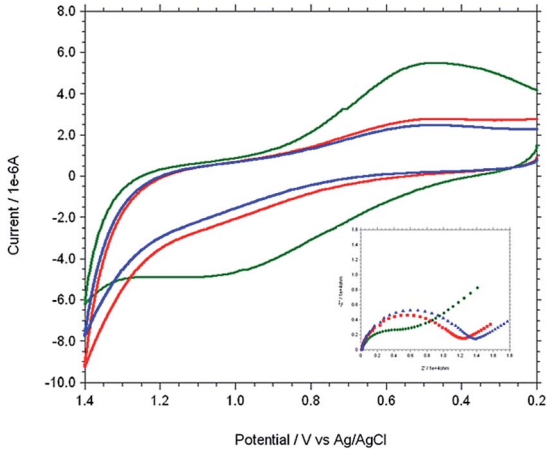

Fig. 8 Overlaid cyclic voltammogram and Nyquist plot ($-Z''$ *versus* Z') (inset) of 1 mM adenine in 0.1 M PBS solution at pH 7 using different working electrode. [bare Au (red), IATP–Au (blue) and Cu^{2+}–IATP–Au (green)].

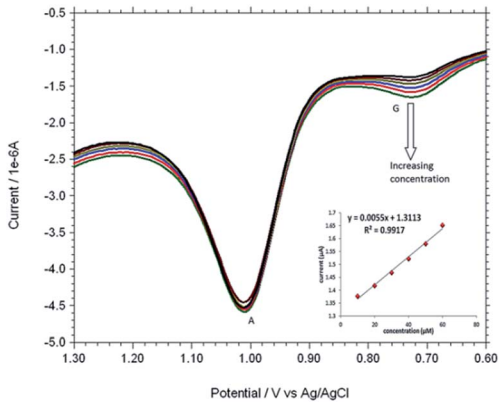

Fig. 9 Overlaid DPV for each increment of 10 μM G to 100 μM A at Cu^{2+}–IATP SAM modified gold electrode in 0.1 M PBS buffer solution at pH 7.0.

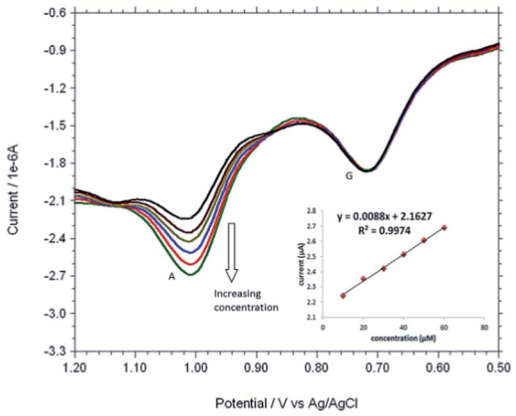

Fig. 10 DPVs obtained for each 10 μM A to 100 μM G at Cu^{2+}–IATP SAM modified gold electrode in 0.1 M PBS buffer solution at pH 7.0.

guanine. It can be seen that the detection limit and linear range of the proposed method are comparable with the reported methods.

3.6. Effect of accumulation time and potential

The effect of accumulation time on the oxidation behaviour of adenine and guanine at Cu^{2+}–IATP–Au electrode was investigated by DPV. Fig. S7(a)† shows that both the oxidation peak current of A and G increased slowly with increasing accumulation time from 0–150 s and thereafter they remain constant. Therefore, an accumulation time of 150 s was chosen as the optimum time for further study. In addition, the influence of accumulation potential on the peak current was examined over the potential range 0.0 to 0.6 V and 0.0 to 0.5 V for adenine and guanine, respectively Fig. 7(b). The peak current decreased by changing accumulation potential to more positive value and is due to the oxidation of A and G during the accumulation step at potential higher than 0.6 V and 0.5 V for adenine and guanine, respectively. In fact, the maximum observed currents were equal to those observed for open circuit accumulation.

3.7. Effect of scan rate and pH

The oxidation peak current of adenine and guanine increased linearly with the scan rate in the range of 10–90 mV s^{-1} (Fig. S8†) following the linear regression equation I_{pa} (μA) = 0.0323 ν (mV s^{-1}) − 0.0624 (R^2 = 0.9939) and I_{pa} (μA) = 0.0393 ν (mV s^{-1}) + 4.7321 (R^2 = 0.9925) for adenine and guanine, respectively. These indicated that the electrooxidation reactions of adenine and guanine at Cu^{2+}–IATP–Au electrode were the surface controlled process. The effect of pH on the electrooxidation of A and G were also investigated in the range of pH 3.0–9.0. As shown in Fig. S9† the oxidation peak potential A and G were pH dependent and that they shifted toward more negative potential with increments in solution pH following the linear regression equation of E_{pa} (V) = −0.059 pH + 1.421 (R^2 = 0.994) and E_{pa} (V) = −0.060 pH + 1.169 (R^2 = 0.993), respectively. The slope of 59.0 and 60.0 mV per pH indicated that equal numbers of protons and electrons were involved in the electrode reaction process.[45] Investigation of the influence of pH on the peak current of purine bases at the modified gold electrode revealed that that peak current of A and G reached a maximum at pH 7.0 and then decreased by increasing pH of the solution (Fig. S9†). On the other hand Cu(II) complexation with azoimidazole on the gold surface (IATP–Au) is maximum at pH 7.0. Considering both results, we have chosen pH 7.0 for the subsequent experiments.

3.8. Interference, reproducibility and stability

The current responses of A and G were studied in presence of some common electroactive interferences such as ascorbic acid, citric acid, cysteine, glucose, Na^+, K^+, Cl^- and SO_4^{2-} in 0.1 M PBS. A 1000 fold excess of ascorbic acid, citric acid, cysteine, glucose, Na^+, K^+, Cl^- and SO_4^{2-} had no effect on the peak

Table 1 Comparative account of different electrochemical sensors for the determination of adenine and guanine[a]

	Adenine		Guanine		
Electrode	Linear range (μM)	Detection limit (μM)	Linear range (μM)	Detection limit (μM)	Reference
GNO–SPAN/CPE	0.5–200	0.05	0.5–200	0.075	10
Pt–Pd/PSi/CNPE	0.1–10	0.03	0.1–10	0.02	12
PPyox/GR/GCE	0.06–100	0.02	0.04–100	0.01	13
MWCNT/$NiFe_2O_4$/GCE	0.1–4.0	0.01	0.05–3.0	0.006	14
AgNPs–Pdop@Gr/GCE	0.02–40	0.002	0.02–40	0.004	15
PSSA–ssDNA/GCE	0.065–1.1	0.02	0.065–1.1	0.02	16
Graphene-COOH/GCE	0.5–200	0.025	0.5–200	0.05	18
4α-Ni^{II}TAPc/GCE	—	—	10–100	0.03	19
FeHCF/GCE	—	—	0–145	0.10	20
Azocalix[4]arene/GCE	0.125–200	0.07	0.125–200	0.05	21
Cu^{2+}–IATP–Au	10–60	0.06	10–60	0.01	This work

[a] GNO: single-layered graphene oxide, SPANI: sulfonated polyaniline, Pt–Pd/Psi: porous silicon supported Pt–Pd nanoalloy, PPyox/GR: overoxidized polypyrrole/graphene, MWCNT/$NiFe_2O_4$: multiwall carbon nanotubes (MWCNTs) decorated with $NiFe_2O_4$ magnetic nanoparticles, AgNPs–Pdop@Gr: Ag nanoparticles (AgNPs)–polydopamine(Pdop)@graphene(Gr)composite, PSSA–ssDNA: poly(sulfosalicylic acid) and single-stranded DNA composite, graphene-COOH: carboxylic acid functionalized graphene, 4α-Ni^{II}TAPc: 1,8,15,22-tetraaminophthalocyanatonickel(II), FeHCF: iron hexacyanoferrate film.

currents of the A and G. A representative DPV is given in Fig. S10† where ascorbic acid was used 1000 fold excess in A and G mixture. The modified electrode shows reproducible results for A and G. The reproducibility of the modified electrode was examined by 8 successive DPV measurements of A and G in PBS solution. The results showed a relative standard deviation (RSD) of 0.5%, indicating that the electrode has good reproducibility. The modified electrode also displays good storage stability if kept in aqueous medium at room temperature over a period of 30 days.

3.9. Real sample analysis

The copper(II) complex modified gold electrode, Cu^{2+}–IATP–Au, was used to determine DNA bases simultaneously in the denatured herring sperm DNA sample. Fig. 11 shows the overlaid DPV of PBS, herring sperm DNA solution and after addition of standard A, G solution in herring sperm DNA solution. The DPV of herring sperm DNA clearly shows four oxidation peaks for four DNA bases. The content of A and G in herring sperm DNA were calculated using the standard addition method and direct interpolation of the linear regression. The results are summarised in Table 2 and agree with the data reported in literature.[21] The accuracy of the method was also verified by recovery studies adding standard DNA base solution to the real sample and 99–100% recoveries were obtained.

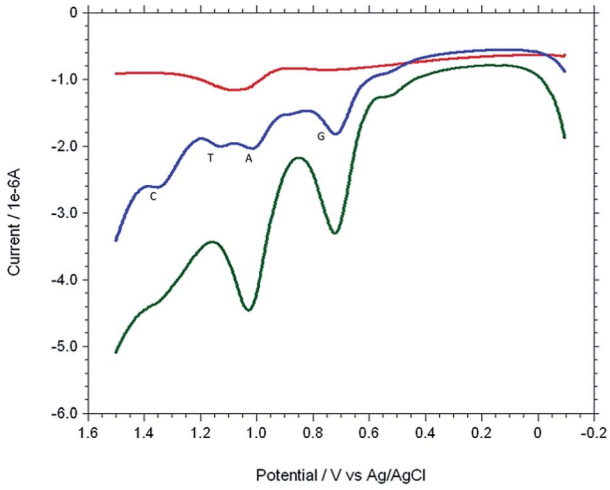

Fig. 11 Overlaid DPVs of 0.1 M PBS solution (red), herring sperm DNA solution (blue) and after addition of standard A, G solution in herring sperm DNA solution (green).

Table 2 Determination of A and G in herring sperm DNA sample with copper(II) complex modified gold electrode

Bases	Detected (μM)	Added (mM)	Found (mM)	Recovery (%)
A	4.4 ± 0.04	1.0	0.99	99.0
G	3.5 ± 0.01	1.0	1.004	100.4

4. Conclusions

A novel electrochemical sensor has been prepared and is used to detect A and G individually, simultaneously in a mixture and in herring sperm DNA. The electrochemical oxidation of A and G was studied using cyclic voltammetry and a prominent anodic oxidation peak was observed using Cu^{2+}–IATP–Au modified electrode. EIS results show the following order of charge transfer resistance: IATP–Au > bare Au > Cu^{2+}–IATP–Au for A and G in PBS (pH 7) and supports the electrocatalytic nature of copper complex modified gold electrode. Distinguishable oxidation peaks of the A and G can be obtained using Cu^{2+}–IATP–Au modified electrode which is very helpful to analyse DNA fragments simultaneously. The modified electrode showed high sensitivity, low detection limit, higher reproducibility and good stability. Moreover, the electrode modification process is easy, economic as well as reproducible. The new sensor can be used for clinical diagnosis and genetic research.

References

1 W. Saenger, in *Principles of Nuclic acid structure*, ed. C. R. Cantor, Springer, New York, 1984; E. Palecek, Electrochemical behaviour of biological macromolecules, *Bioelectrochem. Bioenerg.*, 1986, **15**, 275.
2 H. S. Wang, H. X. Ju and H. Y. Chen, *Anal. Chim. Acta*, 2002, **461**, 243; P. Cekan and S. T. Sigurdsson, *J. Am. Chem. Soc.*, 2009, **131**, 18054.
3 C. C. Carrion, S. Armenta, B. M. Simonet, M. Valcarcel and B. Lendl, *Anal. Chem.*, 2011, **83**, 9391.
4 C. W. Klampfl, M. Himmelsbach, W. Buchberger and H. Klein, *Anal. Chim. Acta*, 2002, **454**, 185; W. R. Jin, H. Y. Wei and X. Zhao, *Electroanalysis*, 1997, **9**, 770.
5 E. B. Liu and B. C. Xue, *J. Pharm. Biomed. Anal.*, 2006, **41**, 649.
6 I. Heisler, J. Keller, R. Tauber, M. Sutherland and H. Fuchs, *Anal. Biochem.*, 2002, **302**, 114.
7 M. Ishikawa, Y. Maruyam, J. Y. Ye and M. Futamata, *J. Lumin.*, 2002, **98**, 81.
8 X. H. Cai, B. Ogorevc and K. Kalcher, *Electroanalysis*, 1995, **7**, 1126; K. J. Ituang, D. J. Niu, J. Y. Sun, C. H. Han, Z. W. Wu, Y. L. Li and X. Q. Xiong, *Colloids Surf., B*, 2011, **82**, 543; J. M. Zen, M. R. Chang and G. Ilangovan, *Analyst*, 1999, **124**, 679.
9 A. Abbaspour and A. Noori, *Analyst*, 2008, **133**, 1664.
10 T. Yang, Q. Guan, Q. Li, L. Meng, L. Wang, C. Liu and K. Jiao, *J. Mater. Chem. B*, 2013, **1**, 2926.
11 A. Abbaspour, M. A. Mehrgardi and R. Kia, *J. Electroanal. Chem.*, 2004, **568**, 261.
12 A. A. Ensafi, M. M. Abarghoui and B. Rezaei, *Sens. Actuators, B*, 2014, **204**, 528.
13 Y.-S. Gao, J.-K. Xu, L.-M. Lu, L.-P. Wu, K.-X. Zhang, T. Nie, X.-F. Zhu and Y. Wu, *Biosens. Bioelectron.*, 2014, **62**, 261.
14 A. A. Ensafi, M. J. Asl, B. Rezaei and A. R. Allafchian, *Sens. Actuators, B*, 2013, **177**, 634.
15 K.-J. Huang, L. Wang, H.-B. Wang, T. Gan, Y.-Y. Wu, J. Li and Y.-M. Liu, *Talanta*, 2013, **114**, 43.

16 L. J. Feng, X.-H. Zhang, P. Liu, H.-Y. Xiong and S.-F. Wang, *Anal. Biochem.*, 2011, **419**, 71.
17 J. Cui, D. Sun, W. Zhou, H. Liu, P. Hu, N. Ren, H. Qin, Z. Huang, J. Lin and H. Ma, *Phys. Chem. Chem. Phys.*, 2011, **13**, 9232.
18 K. J. Huang, D. J. Niu, J. Y. Sun, C. H. Han, Z. W. Wu, Y. L. Li and X. Q. Xiong, *Colloids Surf., B*, 2011, **82**, 543.
19 A. J. Jeevagan and S. A. John, *Anal. Biochem.*, 2012, **424**, 21.
20 S. M. Chen, C. H. Wang and K. C. Lin, *Int. J. Electrochem. Sci.*, 2012, **7**, 405.
21 Q. Xu, X. Liu, H. Li, L. Yin and X. Hu, *Biosens. Bioelectron.*, 2013, **42**, 355.
22 H. Yin, Y. Zhou, Q. Ma, S. Ai, P. Ju, L. Zhu and L. Lu, *Process Biochem.*, 2010, **45**, 1707.
23 R. N. Goyal, V. K. Gupta, M. Oyama and N. Bachheti, *Talanta*, 2007, **71**, 1110.
24 X. Xie, K. Zhao, X. Xu, W. Zhao, S. Liu, Z. Zhu, M. Li, Z. Shi and Y. Shao, *J. Phys. Chem. C*, 2010, **114**, 14243.
25 E. Radi, X. M. Berbel, M. C. Puig and J. L. Martyc, *Electroanalysis*, 2009, **21**, 696; L. S. Jiao, L. Niu, J. Shen, T. Y. You, S. J. Dong and A. Ivaska, *Electrochem. Commun.*, 2005, **7**, 219.
26 G. T. Hermenson, *Bioconjugate Techniques*, Academic Press, San Diego, CA, 2nd edn, 2008; F. Li, Y. Feng, P. Dong and B. Tang, *Biosensors Bioelectronics*, 2010, **25**, 2084.
27 Sk. Jasimuddin, *Transition Met. Chem.*, 2006, **31**, 724; Sk. Jasimuddin and C. Sinha, *Transition Met. Chem.*, 2004, **29**, 566.
28 L. Trnkova, L. Zerzankova, F. Dycka, R. Mikelova and F. Jelen, *Sensors*, 2008, **8**, 429.
29 K. Barman and Sk. Jasimuddin, *Indian J. Chem., Sect. A: Inorg., Bio-inorg., Phys., Theor. Anal. Chem.*, 2013, **52**, 217.
30 R. K. Shervedani, F. Yaghoobi, A. H. Mehrjardi and S. M. S. Barzoki, *Electrochim. Acta*, 2008, **53**, 4185.
31 S. Y. M. Shikov, A. V. Vurasko, L. S. Molechmikov, E. G. Kovalyova and A. A. Ffendieu, *J. Mol. Catal. A: Chem.*, 2000, **158**, 447.
32 Z. Dursun, I. Sahbaz, F. N. Ertas and G. Nisli, *Turk. J. Chem.*, 2003, **27**, 513.
33 Z. Zhang, X. Li, C. Wang, C. Zhang, P. Liu, T. Fang, Y. Xiong and W. Xu, *Dalton Trans.*, 2012, **41**, 1252.
34 T. Rohani and M. A. Taher, *Talanta*, 2009, **78**, 743.
35 K. Kano, M. Torimura, Y. Esaka and M. Goto, *J. Electroanal. Chem.*, 1994, **372**, 137.
36 B. J. Sanghavi, S. M. Mobin, P. Mathur, G. K. Lahiri and A. K. Srivastava, *Biosens. Bioelectron.*, 2013, **39**, 124.
37 J. F. Smalley, K. Chalfant, S. W. Feldberg, T. M. Nahir and E. F. Bowden, *J Phys. Chem. B*, 1999, **103**, 1676.
38 R. K. Shervedani, A. Hatefi-Mehrjardi and M. Khosravi Babadi, *Electrochim. Acta*, 2007, **52**, 7051 and references therein.
39 G. G. Hammes, *Enzyme catalysis and regulation*, Academic, New York, 1982; T. Palmer, *Understanding Enzymes*, Ellis. Horwood, Chicester, 2nd edn, 1985; G. N. Mukherjee and A. Das, *Elements of Bioinorganic Chemistry*, U. N. Dhur & Sons Pvt. Ltd, Kolkata, 1st edn, 1993.
40 R. K. Shervedani, S. M. S. Barzoki and M. Bagherzadeh, *Electroanalysis*, 2010, **22**, 969.
41 S. Campuzano, M. Pedrero, C. Montemayor, E. Fatas and J. M. Pingarron, *J. Electroanal. Chem.*, 2006, **586**, 112.
42 Q. Li, C. Batchelor-McAuley and R. G. Compton, *J. Phys. Chem. B*, 2010, **114**, 7423; L. M. Goncalves, C. Batchelor-McAuley, A. A. Barros and R. G. Compton, *J. Phys. Chem. C*, 2010, **114**, 14213.
43 Y. Wei, Q. A. Huang, M. G. Li, X. J. Huang, B. Fang and L. Wang, *Electrochim. Acta*, 2011, **56**, 8571–8575.
44 P. N. Mashazi, P. Westbroek, K. I. Ozoemena and T. Nyokong, *Electrochim. Acta*, 2007, **53**, 1858.
45 E. Laviron, *J. Electroanal. Chem.*, 1974, **52**, 355.

RSC Advances

COMMUNICATION

Cite this: *RSC Adv.*, 2016, **6**, 20800

Received 12th December 2015
Accepted 12th February 2016

DOI: 10.1039/c5ra26534g

www.rsc.org/advances

Non-enzymatic electrochemical sensing of glucose and hydrogen peroxide using a bis(acetylacetonato)oxovanadium(IV) complex modified gold electrode†

Koushik Barman and Sk Jasimuddin*

A non-enzymatic electrochemical sensor, bis(acetylacetonato)oxovanadium(IV) complex, $[VO(acac)_2]$, fabricated on a self-assembled 4-(pyridine-4′-amido)thiophenol (PATP) monolayer modified gold electrode, was developed for the detection of glucose and hydrogen peroxide (H_2O_2) at neutral pH. The modified electrode was characterized by electrochemical and microscopic techniques. The non-enzymatic sensor exhibited a remarkable catalytic performance for glucose oxidation and H_2O_2 reduction. Chronoamperometry was used for the electrochemical determination of glucose and H_2O_2. The non-enzymatic sensing of glucose was realized with a linear response range from 0.001 to 0.5 mM with a detection limit of 0.1 μM (S/N = 3). The sensor also has a good performance for the electrocatalytic reduction of H_2O_2 with a linear response range from 0.02 to 0.9 mM with a detection limit of 0.03 μM (S/N = 3). In addition, $[VO(acac)_2]$–PATP–Au showed a good selectivity for glucose and H_2O_2 detection in the presence of potential interfering agents such as ascorbic acid, uric acid, L-dopa, L-cysteine and different ions like Na^+, K^+, Cl^- *etc.* The kinetic parameters such as the electron transfer coefficient and the catalytic reaction rate constant were also determined for glucose and H_2O_2. Finally, the modified electrode was used to achieve quantitative detection of glucose and H_2O_2 in blood and milk, respectively for practical applications.

Introduction

Green plants produce glucose by the reduction of carbon dioxide and the metabolic oxidation of glucose sustains all living beings.[1] Glucose is transported to cells *via* insulin in the bloodstream. The human body maintains blood glucose levels at a concentration of 4–8 mM (70–120 mg dL^{-1}).[2] An abnormal blood sugar level causes diabetes which represents a leading cause of several complications for human health like complications to the retina, circulatory system, kidneys *etc.*[3] To manage the blood glucose level patients need to monitor the blood glucose level on a regular basis. On the other hand, hydrogen peroxide (H_2O_2) is a simple but very important molecule in nature, and is extensively used as an oxidizing agent in the food and chemical industries.[4] Moreover, H_2O_2 is one of the most important markers for oxidative stress and also acts as a precursor in the formation of highly reactive and potentially harmful hydroxyl radicals.[5,6] Therefore, the accurate determination of glucose and H_2O_2 is of practical importance. Several analytical techniques have been carried out for the determination of glucose and H_2O_2 *viz.*, titrimetry, spectrometry, fluorometry, chemiluminescence and electrochemical methods.[7–10] Amongst them, the electrochemical approach is promising because of its higher sensitivity and selectivity, lower detection limit, faster response time, better long term stability and chip.[11] For the detection of glucose and H_2O_2 both enzymatic[12,13] and non-enzymatic[14,15] sensor have been developed. First, second and third generation enzymatic glucose sensors has been developed due to overcome the disadvantages. The third generation sensor still in their infancy, yet some of them based on nano-mesoporous electrode surface show some promise.[16] There are still some disadvantages of enzyme-based determination. Examples include complicated enzyme immobilization, critical operating conditions *viz.* optimum temperature and pH, chemical instability, poor reproducibility and high cost.[17] To solve these problems, fourth generation enzyme-free sensors have been developed for glucose oxidation and H_2O_2 reduction. In general, these electroactive analytes can be oxidized or reduced directly at ordinary solid electrodes. However, owing to their high over-potential, slow electrode kinetics and poor measurement stability caused by poisoning from the intermediate products restricts the performance of this electrodes.[18] Therefore; current efforts have mainly focused on discovering new materials with high catalytic activity and good stability in order to construct non-enzymatic sensors. The fabrication of a wide variety of nanomaterials have been introduced for the selective and sensitive detection of glucose[19,20] as well as H_2O_2.[21,22] On the other hand very limited numbers of

Department of Chemistry, Assam University, Silchar, Assam-788011, India. E-mail: j.seikh@gmail.com

† Electronic supplementary information (ESI) available: Figures, table *etc.* See DOI: 10.1039/c5ra26534g

metal complexes have been used so far for the electrochemical sensing of glucose and H_2O_2. Complexes with reversible redox capabilities such as cobalt phthalocyanine,[23] nickel curcumin,[24] nickel porphyrine,[25] copper hexacyanoferrate[26] have been used for the effective electrocatalytic sensing for glucose whereas cobalt tetrasulfophthalocyanine,[27] cobalt tetraruthenated porphyrin,[28] cobaltoxyhydroxide,[22] DNA–Cu^{2+} complex[29] for H_2O_2 sensing.

Instead of cobalt, nickel and copper containing complexes no other earth abundant transition metal complexes have been reported for the electrochemical sensing of glucose and H_2O_2. Among first d-block transition-metal series, vanadium has critical roles in various chemical and biological processes.[30] Presently the catalytic role of vanadium in higher oxidation states (IV and V) has received much attention after the discovery of vanadium dependent enzymes such as vanadiumiron nitrogenase of *Azotobacter vinelandii* and vanadium haloperoxidases in marine algae.[31] Several oxovanadium and dioxovanadium complexes acts as functional models of haloperoxidases and catalyze oxyhalogenation of various aromatic substrates.[32] Instead of these, oxovanadium complexes have also been used to catalyze several reactions such as the oxidation of olefins, alcohols,[33] aldehydes,[34] tertiary amine,[35] thiols,[36] hydrogen peroxide,[37] epoxidation[38] and oxidative coupling reaction.[39] Apart from their role as catalyst, there is a widespread interest on the biological chemistry of vanadium compounds because of its perceived potential for the development as a pharmacologic agent for the treatment of diabetes mellitus.[40] Extensive literature review shows that among large number of oxovanadium compounds, only bis(acetylacetonato)oxovanadium, $[VO(acac)_2]$, exhibits the greatest capacity to enhance insulin receptor kinase activity in cells associated with a significant decrease in plasma glucose concentration.[41] Posner and co-workers showed that vanadate reacted with H_2O_2 stimulated the phosphorylation of the insulin receptor in endosomes with efficiency comparable to that of insulin.[42] Makinen and Brady showed that $[VO(acac)_2]$ stimulate the uptake of glucose by serum-starved 3T3-L1 adipocytes in the presence of bovine serum albumin.[43]

These rich catalytic and pharmacological properties of oxovanadium complexes encourage us to prepare the $[VO(acac)_2]$ complex modified gold electrode and study the non-enzymatic electrochemical sensing behaviour for glucose and hydrogen peroxide. To the best of our knowledge, this is the first report of sensing both glucose and hydrogen peroxide by the same metal complex modified electrode at neutral pH. The oxovanadium(IV) complex modified gold electrode shows excellent electrocatalytic activity and exhibit notable sensing performance towards glucose and H_2O_2. The kinetics of glucose oxidation and hydrogen peroxide reduction was also examined in detail. More importantly, we demonstrate successfully its application for the quantitative detection of glucose in human blood sample and H_2O_2 in processed milk.

Experimental

Chemicals and reagents

4-Aminothiophenol, isonicotinic acid, $[VO(acac)_2]$, D-(+)-glucose and hydrogen peroxide (30 wt% in H_2O) were procured from Sigma Aldrich, India, $K_4[Fe(CN)_6]_3 \cdot H_2O$ were purchased from Merck (India). All the reagents and solvents were analytical grade and were used without further purification. 0.1 M phosphate buffer solution (PBS) was prepared by mixing 0.1 M $NaClO_4$ and 0.01 M H_3PO_4 and the pH's were adjusted by the addition of 0.11 M NaOH using Smalley's method.[44] Double distilled water was used throughout the course of the experiment.

Apparatus and instrumentations

Electrochemical measurements were performed on a CHI 660C Electrochemical workstation (CH Instrument, USA). A three electrode system was employed with gold or modified gold electrode as working electrode (2 mm diameter, 0.031 cm^2 area), Pt wire as a counter electrode and Ag/AgCl (3 M KCl) as reference electrode. All experiments were performed at ambient temperature and inert atmosphere. The field emission scanning electron microscopy (FE-SEM) images were obtained using FE SEM, FEI INSPECT F50 operated at an acceleration voltage of 20 kV. pH measurement of solutions were carried out on a pH meter (Macro Scientific Works (Regd), New Delhi).

Construction of $[VO(acac)_2]$–PATP modified gold electrode

A gold electrode was polished with wet α-alumina (0.5 μm) on a flat polishing pad for 10 minutes and rinsed several times with doubly distilled water. The cleanliness of the gold electrode surface was ascertained by recording the repetitive cyclic voltammograms in 0.5 M H_2SO_4 between −0.2 and +1.5 V *versus* Ag/AgCl with 0.1 V s^{-1} scan rate until a steady characteristic gold oxide cyclic voltammogram was obtained.[45] The electrode was then rinsed with doubly distilled water and immersed in 1.0 mM ethanolic solution of 4-aminothiophenol (4-ATP) for 24 hours. The 4-ATP was self-assembled over the gold electrode surface *via* gold–sulfur interaction and the modified electrode 4-ATP–Au was thoroughly washed with double distilled water. Thereafter, the modified gold electrode was dipped into 1.0 mM isonicotinic acid solution for 4 hours under stirring condition and 4-(pyridine-4′-amido)thiophenol modified gold electrode (PATP–Au) was formed. After washed with double distilled water PATP–Au electrode was immersed into an ethanolic solution of 1.0 mM $[VO(acac)_2]$ and stirred for 2 hours so that the pyridine nitrogen of PATP–Au was able to form adduct with the vacant coordination site of vanadium in $[VO(acac)_2]$. The finally modified electrode $[VO(acac)_2]$–PATP–Au was washed thoroughly with distilled water and dried in air for further use.

Results and discussion

Characterization of modified gold electrode

The step wise modification and surface morphology of the bare gold electrode was characterised by FE-SEM. $[VO(acac)_2]$–PATP modified gold electrode shows very rough and porous surface which is favourable for the electrocatalytic activity. Elemental mapping images confirms the immobilization of $[VO(acac)_2]$ over self-assembled monolayer 4-PATP modified gold electrode.[46] The modification process was also monitored by cyclic

voltammetry and electrochemical impedance spectroscopy using $[Fe(CN)_6]^{3-/4-}$ as redox probe in 0.1 M PBS solution at pH 7.0. The cyclic voltammogram of 0.5 mM $[Fe(CN)_6]^{4-}$ exhibits an electrochemically reversible redox couple on bare electrode. After modification the gold electrode with 4-aminothiophenol, the cyclic voltammogram of $[Fe(CN)_6]^{4-}$ exhibit an irreversible couple with low current height than bare gold electrode. The current height decreased even more when 4-(pyridine-4′-amido) thiophenol (PATP) modified Au was used as working electrode. These CV results indicated that the electronic communication between gold and $[Fe(CN)_6]^{4-}$ is blocked due to PATP film formation.[46] In the Nyquist plot, the diameter of the semi-circle increases gradually when stepwise modification on the gold electrode surface was carried out. The observed trend is due to the fact that the modified electrode blocked the electron transfer for the redox reaction of $[Fe(CN)_6]^{4-}$. Electrochemical impedance measurement supports the CV results. The fabrication of $[VO(acac)_2]$ over PATP–Au electrode was confirmed by taking a comparative cyclic voltammogram for PATP–Au and $[VO(acac)_2]$–PATP–Au in 0.1 M PBS buffer at pH 7.0. A quasi-reversible $[V^{V}O(acac)_2]^{+}/[V^{IV}O(acac)_2]$ redox couple at +0.33 V supports the fabrication of $[VO(acac)_2]$–4-PATP–Au electrode.[46]

Electrocatalytic oxidation of glucose and reduction of H_2O_2

Fig. 1 and 2 shows the cyclic voltammograms (CV) of 0.1 mM glucose and 0.5 mM hydrogen peroxide, respectively in 0.1 M PBS at pH 7.0 using bare Au, PATP–Au and $[VO(acac)_2]$–PATP–Au electrodes. An irreversible oxidation of glucose occurred at +0.65 V by the $[VO(acac)_2]$–PATP–Au electrode with large increase of current whereas no such prominent peak was observed with bare and PATP–Au electrode (Fig. 1). In absence of glucose no such oxidation peak was observed at $[VO(acac)_2]$–PATP–Au electrode (Fig. S1†). This behaviour indicate the electrocatalytic activity of $[VO(acac)_2]$–PATP modified gold electrode towards glucose oxidation. DPV experiment gives a prominent glucose oxidation peak only at $[VO(acac)_2]$–PATP–Au electrode under similar condition and supports the results obtained by CV (Fig. S2†). The catalytic pathway of glucose oxidation can be describe on assuming that the electrochemical process is

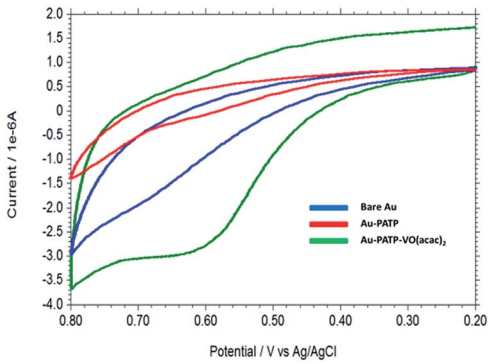

Fig. 1 Cyclic voltammograms obtained with bare, PATP and $[VO(acac)_2]$–PATP modified gold electrode in 0.1 mM glucose in 0.1 M PBS solution (pH 7.0).

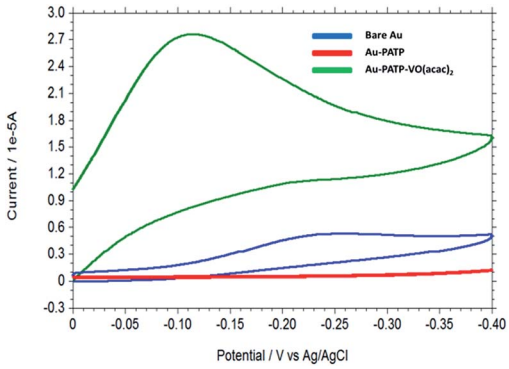

Fig. 2 Cyclic voltammograms obtained with bare, PATP and $[VO(acac)_2]$–PATP modified gold electrode in 0.5 mM hydrogen peroxide in 0.1 M PBS solution (pH 7.0).

initiated by the non-covalent interaction of glucose with surface bound $[VO(acac)_2]$. During anodic scan $[V^{IV}O(acac)_2]^0$ is oxidized to the catalytically active $[V^{V}O(acac)_2]^+$ complex over PATP modified gold electrode.

$$[V^{IV}O(acac)_2]^0 \rightarrow [V^{V}O(acac)_2]^+ + e^-. \quad (a)$$

Once $[V^{V}O(acac)_2]^+$ is formed, glucose is oxidized on the modified electrode surface *via* the following reactions.

$$[V^{V}O(acac)_2]^+ + \text{glucose} \rightarrow \text{intermediate} + [V^{IV}O(acac)_2]^0 \quad (b)$$

$$[V^{V}O(acac)_2]^+ + \text{intermediate} \rightarrow \text{gluconolactone} + [V^{IV}O(acac)_2]^0. \quad (c)$$

The cyclic voltammogram of H_2O_2 in 0.1 M PBS (pH 7.0) shows a cathodic response at around −0.24 V at bare gold electrode. When the gold electrode was modified by 4-(pyridine-4′-amido)thiophenol, no current response was observed. After modification with $[VO(acac)_2]$, a sharp peak was observed around −0.11 V with sufficiently high current response during the cathodic scan. In absence of H_2O_2 no such reduction peak was obtained at $[VO(acac)_2]$–PATP–Au electrode under similar condition (Fig. S3†). Through these observations it was clear that oxovanadium(IV) complex exhibit enhanced electrocatalytic efficiency by their adhesion on the PATP–Au electrode. This is rationalized by a high ability of the $[VO(acac)_2]$ to transfer electrons involved in the catalytic reaction and sense the presence of H_2O_2 electrochemically. A common two electron redox mechanism is proposed for hydrogen peroxide reduction at the $[VO(acac)_2]$–PATP–Au electrode surface in which a substantial interaction with H_2O_2 and vanadium promotes the electron transfer and is shown by the following reactions.

$$[V^{IV}O(acac)_2]^0 + H_2O_2 \rightarrow H_2O + [V^{V}O(acac)_2]^+ \quad (d)$$

$$[V^{V}O(acac)_2]^+ + e^- \rightarrow [V^{IV}O(acac)_2]^+ \quad (e)$$

Electrochemical impedance spectroscopy was also carried out for glucose and H_2O_2 using bare and modified gold

electrodes. The diameter of the semicircle observed in the Nyquist plot corresponds to charge transfer resistance, R_{ct}; the smaller the semi-circle, faster is the charge transfer. Fig. S4 and S5† shows that the diameter of the semicircle (R_{ct}) changes upon modification of gold electrode surface. The R_{ct} values for 0.1 mM glucose oxidation and 0.5 mM H_2O_2 reduction at $[VO(acac)_2]$–4-PATP–Au electrode in 0.1 M PBS at pH 7.0 were 1.3 $\times$ 10^4 Ω and 1.2 $\times$ 10^5 Ω respectively, which were quite smaller than the R_{ct} obtained at PATP modified and bare gold electrode. The observed results are due to the fact that the $[VO(acac)_2]$-modified electrode ease the electron transfer rate for the oxidation of glucose and reduction of H_2O_2 where as the 4-PATP modified gold electrode blocked the electron transfer. Electrochemical impedance measurements clearly indicate that $[VO(acac)_2]$–4-PATP modified gold electrode has lower resistance as compared to bare or 4-PATP modified gold electrodes. This study supports the CV results and reveals that the $[VO(acac)_2]$–4-PATP–Au electrode is an efficient electrocatalyst for the oxidation of glucose and reduction of hydrogen peroxide.

Determination of glucose and H_2O_2

Based on optimized conditions, determination of glucose and H_2O_2 were performed using chronoamperometry. Fig. S6† shows the chronoamperometry curves of glucose with different concentration. The oxidation peak current of glucose was linear with its concentration in the range of 0.1–0.5 mM (Fig. 3a). The regression equation was $I = 3.717C + 1.646$ ($R^2 = 0.99$), with a detection limit of 0.1 μM (S/N = 3). Exactly same detection limit was obtained in the lower concentration range of glucose (1.0 μM to 5.0 μM) (Fig. S8†). The detection limit was further confirmed by differential pulse voltammetry (Fig. S10†). Fig. S7 and S9† shows the chronoamperogram response for H_2O_2 in the concentration range of 0.5–0.9 mM and 20–40 μM. The current was linearly proportional to its higher concentration range with a linear regression equation $I = 9.81C + 18.61$ ($R^2 = 0.99$) (Fig. 3b) and in the low concentration range with a linear regression equation $I = 9.81C + 0.02$ ($R^2 = 0.99$) (Fig. S9b†). The detection limit for H_2O_2 was 0.03 μM (S/N = 3). The detection limit was further confirmed using CV results (Fig. S11†). Table S1† shows a comparison of the proposed electrochemical method and other modified electrodes reported for the electrocatalytic oxidation of glucose and reduction of H_2O_2. It can be seen that the detection limit obtained in the present system are comparable with some reported metal complex modified electrodes and quite better than the metal nanoparticle/nanocomposite modified electrodes.

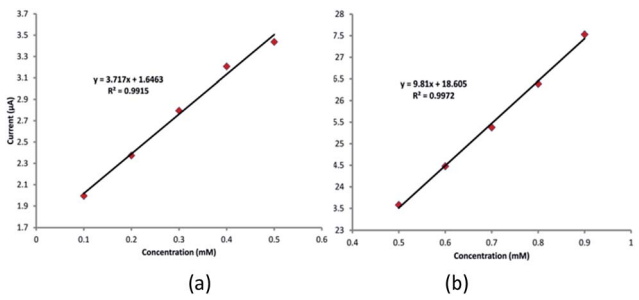

Fig. 3 (a) Plot of resulting current in chronoamperometry at 30 seconds *versus* concentration of glucose (0.1–0.5 mM). (b) Plot of resulting current in chronoamperometry at 30 seconds *versus* concentration of H_2O_2 (0.5–0.9 mM).

Effect of scan rate and kinetic analysis for glucose oxidation and hydrogen peroxide reduction

The influence of the scan rate on the electrocatalytic oxidation of glucose (Fig. S12a†) and the reduction of H_2O_2 (Fig. S13a†) at $[VO(acac)_2]$–4-PATP–Au were investigated using cyclic voltammetry. The results showed that on increasing the scan rates the oxidation peak potential of glucose and the reduction potential of hydrogen peroxide shifts to more positive and more negative values, respectively, confirming the kinetic limitation of the electrochemical reaction.[27] Moreover, a plot of scan rate–normalized current ($I_{pa}/\nu^{1/2}$) *versus* scan rate (Fig. S14†) shows a shape typical of EC catalytic process for glucose oxidation.[47] In addition, a plot of the peak current (I_{pa}) *versus* the square root of the scan rate ($\sqrt{\nu}$) (Fig. S12b†) in the range of 50–100 mV s^{-1} was found to be linear following the linear regression equation I_{pa} (μA) = 0.3392ν (mV s^{-1}) − 1.1978 ($R^2 = 0.9945$), revealing that the electrooxidation reaction of glucose at $[VO(acac)_2]$–4-PATP–Au electrode was followed diffusion controlled electron transfer process. The diffusion coefficient (D) for glucose was 9.5 $\times$ 10^{-6} cm^2 s^{-1} and is calculated using the plot (I_{pa} *vs.* $\sqrt{\nu}$) and Randles–Sevcik equation[48]

$$I_p = 2.69 \times 10^5 n^{3/2} A D^{1/2} C \nu^{1/2} \quad (1)$$

where, I_p is the peak current, n is the number of electrons transferred, A is the electrode area, C is the concentration of electroactive species, and ν is the scan rate, considering a temperature of 298 K. The electron transfer coefficient for the totally irreversible oxidation of glucose at $[VO(acaca)_2]$–4-PATP–Au can be determined from equation[48]

$$E_p - E_{p/2} = 1.857RT/\alpha F = 47.7/\alpha \text{ mV} \quad (2)$$

where E_p and $E_{p/2}$ represent the peak potential and the half-height peak potential, respectively in cyclic voltammetry experiment where R, T and F have their usual meaning. For glucose oxidation, $E_p - E_{p/2}$ = 38 mV, hence electron transfer coefficient (α) is calculated to be 0.63.

The standard heterogeneous rate constant (k_s) for the irreversible oxidation of glucose at $[VO(acac)_2]$–4-PATP–Au electrode was calculated by using the Velasco equation[49]

$$k_s = 1.11 D^{1/2} (E_p - E_{p/2})^{-1/2} \nu^{1/2} \quad (3)$$

The estimated k_s values for totally irreversible oxidation of glucose at $[VO(acac)_2]$ modified electrodes was found to be 5.5 $\times$ 10^{-3} cm s^{-1}. The observed higher k_s value for glucose at the modified electrode indicates that the oxidation of glucose was faster at the $[VO(acac)_2]$–PATP modified gold electrode. The kinetic parameters for the reduction of H_2O_2 were also

calculated (as described for glucose): $n = 2$, $\alpha = 0.69$, $D = 10.6 \times 10^{-6}$ cm^2 s^{-1} and $k = 3.3 \times 10^{-3}$ cm s^{-1}.

Effect of accumulation potential and time

The effect of accumulation time and potential on the oxidation behavior of glucose and reduction of H_2O_2 at [VO(acac)$_2$]–PATP–Au electrode was investigated. Fig. S15† shows that the oxidation peak current of glucose and H_2O_2 which were remaining constant with increasing accumulation time from 0 to 300 s. Therefore the accumulation time of 60 s was chosen as the optimum time for further study in both cases. In addition, the influence of accumulation potential on the peak current was examined over the potential range 0.0 to 6.0 V for glucose and 0.0 to −0.5 V for H_2O_2 (Fig. S16†). The peak current for glucose was decreased by changing accumulation potential to more positive value and is due to the oxidation of glucose during the accumulation step at potential higher than that 0.35 V (Fig. S16a†) where as in case of H_2O_2, by changing accumulation potential to more negative value and is due to the reduction of H_2O_2 during the accumulation step at potential lower than that −0.02 V (Fig. S16b†). In fact, the maximum observed current were equal to those observed for open circuit accumulation.

Effect of pH

The effect of pH on the electrooxidation of glucose and H_2O_2 ware also investigated in the range of pH 5.0–10.0. As shown in Fig. S17† the oxidation peak potential of glucose were pH dependent and was shifted towards more negative potential with increments in solution pH following the linear regression equation of E_{pa} (V) = −0.0625 pH + 1.094 (R^2 = 0.9957). The slope of 62.5 mV pH^{-1} indicated that equal numbers of protons and electrons were involved in the electrode reaction process.[50] Similarly, in Fig. S18† the reduction peak potential of H_2O_2 were also pH dependent and that they shifted toward more positive potential with increments in solution pH following the linear regression equation of E_{pa} (V) = −0.026 pH + 0.068 (R^2 = 0.976). Investigation of the influence of pH on the peak current of glucose and H_2O_2 at the modified electrode revealed that peak current of glucose and hydrogen peroxide reached a maximum at pH 7.0 and then decreased by increasing pH of the solution (Fig. S19a and b†).

Reproducibility, sensitivity and stability

A reproducible and long-term stable electrochemical sensor is highly desirable for the practical application and commercialization. The reproducibility of the [VO(acac)$_2$]–PATP–Au electrode was examined by 10 repetitive measurements for glucose and H_2O_2 in 0.1 M PBS solution. The results showed that the anodic peak current for glucose and cathodic peak current for hydrogen peroxide remains same with a relative standard deviation (RSD) of 0.2 and 0.3%, respectively, indicating that the modified electrode has a good reproducibility. The modified electrode was highly sensitive towards glucose and H_2O_2 and the sensitivity was 120.24 μA cm^{-2} mM^{-1} and 326.66 μA cm^{-2} mM^{-1} for glucose and hydrogen peroxide, respectively. To further explore the long-term stability, measurements were made with five days intervals (when not in use, the sensor was stored at room temperature using a rubber cap). The sensor retained 100% of its original current response after 20 days both for glucose (1.0 mM) and H_2O_2 (0.5 mM) in 0.1 M PBS at [VO(acac)$_2$]–PATP–Au (Fig. S20†).

Interference study

In the electrochemical detection of glucose and H_2O_2, the elimination of interferences is a real challenge. Ascorbic acid, uric acid, citric acid, levodopa, cysteine, and different common ions are the major potential interfering agents in the physiological system. In the present study 0.1 mM glucose in presence of 10 fold excess interferents were used at +0.65 V. The resulting amperograms are shown in Fig. 4. There is no obvious current response observed with the addition of these interfering substances, however, an obvious current response with the addition of glucose was appeared. In addition, the influence of those co-existing electroactive species in the amperometric determination of H_2O_2 was also studied. The working potential was held at −0.11 V. The amperogram (Fig. 5) shows that all the potential interferents mentioned did not affect the sensor selectivity for H_2O_2. These results suggest that the interfering effect caused by these electroactive species is quite negligible, indicating the highly selective detection of glucose and H_2O_2 at the oxovanadium complex modified electrode.

Real sample analysis

To testify the feasibility of [VO(acac)$_2$]–PATP–Au in real sample analysis, human blood sample (after fasting) was taken for glucose determination whereas processed milk was chosen for the determination of H_2O_2. Before testing, the blood and milk samples were half diluted by 0.1 M phosphate buffer solution.

Fig. S21† shows the overlaid DPV of blood sample solution in PBS (pH 7.6) and after addition of standard glucose solution in blood sample solution. The DPV of blood sample clearly shows the oxidation of glucose at +0.56 V. The content of glucose in

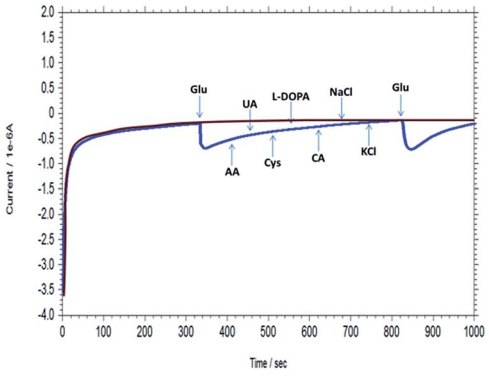

Fig. 4 Amperometric response at [VO(acac)$_2$]–4PATP–Au electrode with an applied potential of +0.65 V on subsequent addition of 0.1 mM glucose, 1.0 mM AA, 1.0 mM UA, 1.0 mM Cys, 1.0 mM L-dopa, 1.0 mM CA, 1.0 mM NaCl, 1.0 mM KCl, 0.1 mM glucose under stirring condition (supporting electrolyte: 0.1 M PBS (pH 7.0), brown curve shows background current).

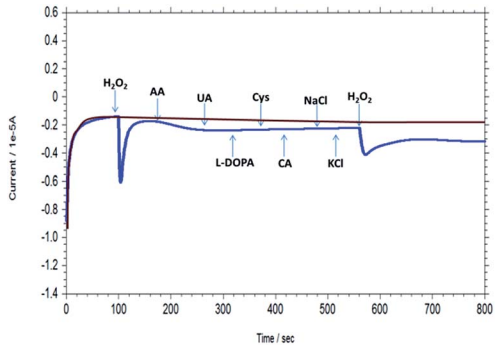

Fig. 5 Amperometric response at $[VO(acac)_2]$–4PATP–Au with an applied potential of −0.11 V on subsequent addition of 0.1 mM H_2O_2, 1.0 mM AA, 1.0 mM UA, 1.0 mM L-dopa, 1.0 mM Cys, 1.0 mM CA, 1.0 mM NaCl, 1.0 mM KCl, 0.05 mM H_2O_2 under stirring condition (supporting electrolyte: 0.1 M PBS (pH 7.0), brown curve shows background current).

blood sample (5.01 mM = 90.258 mg dL^{-1}) was calculated using the standard addition method and the direct interpolation of the linear regression (RSD = 2.24%). A normal fasting (no food for eight hours) blood sugar level is between 70 and 99 mg dL^{-1} and by comparing our result was in the similar range. The accuracy of the method was also verified by recovery studied adding standard glucose solution to the real sample and 100.2% recoveries were obtained. The H_2O_2 concentration in the milk sample was determined as 0.91 μM (= 0.003 mg dL^{-1}), using a standard addition method (RSD = 2.16%), with the recovery of 101.0%. The results are summarized in Table S2.† The results indicate that the modified electrode can effectively detect glucose in human blood and hydrogen peroxide in processed milk.

Conclusions

A unique non-enzymatic electrochemical sensor $[VO(acac)_2]$–PATP–Au was developed and used for the detection of glucose and hydrogen peroxide in pure, presence of interferents and real sample. The modified electrode was characterized by microscopic and electrochemical techniques. Cyclic voltammetry, differential pulse voltammetry, electrochemical impedance spectroscopy, amperometry, chronoamperomery was used for sensing, quantification and determination of kinetic parameters. Till date very limited number of transition metal complex modified electrode has been used for non-enzymatic sensing of glucose and hydrogen peroxide. The novelty of our work is that the same oxovanadium complex modified electrode can detect both glucose as well as hydrogen peroxide. Only few nanoparticles modified electrode has been reported those are able to detect both glucose and hydrogen peroxide. But their preparation process, stability, detection limit, cost are not so impressive. The advantage of our system are easy to prepare, have good selectivity, sensitivity, stability, reproducibility, low detection limit and most importantly cheap than the earlier reported systems. The sensor was efficiently detected glucose in blood sample and hydrogen peroxide in processed milk with good recovery. The new non-enzymatic sensor can be useful for clinical diagnosis and food industry in near future.

References

1 T. Audesirk and G. Audesirk, *Biology, Life on Earth*, Prentice-Hall, 5th edn, 1999.
2 *Medical Instrumentation Application and Design*, ed. J. Webster, Wiley, Hoboken, NJ, 4th edn, 2009.
3 B. J. Privett, J. H. Shin and M. H. Schoenfisch, *Anal. Chem.*, 2008, **80**, 4499.
4 M. Zhou, Y. Zhai and S. Dong, *Anal. Chem.*, 2009, **81**, 5603.
5 M. Giorgio, M. Trinei, E. Migliaccio and P. G. Pelicci, *Nat. Rev. Mol. Cell Biol.*, 2007, **8**, 722.
6 C. Laloi, K. Apel and A. Danon, *Curr. Opin. Plant Biol.*, 2004, **7**, 323.
7 N. V. Klassen, D. Marchington and H. C. E. McGowan, *Anal. Chem.*, 1994, **66**, 2921.
8 Z. H. Li, D. H. Li, K. Oshita and S. Motomizu, *Talanta*, 2010, **82**, 1225.
9 T. Jiao, B. D. Leca-Bouvier, P. Boullanger, L. J. Blum and A. P. Girard-Egrot, *Colloids Surf., A*, 2008, **321**, 143.
10 B. Haghighi and S. Bozorgzadeh, *Microchem. J.*, 2010, **95**, 192.
11 Y. Shen, M. Trauble and G. Wittstock, *Anal. Chem.*, 2008, **80**, 750.
12 S. H. Lim, J. Wei, J. Lin, Q. Li and J. KuaYou, *Biosens. Bioelectron.*, 2005, **20**, 2341.
13 M.-Y. Hua, Y.-C. Lin, R.-Y. Tsai, H.-C. Chen and Y.-C. A. Liu, *Microchim. Acta*, 2011, **56**, 9488.
14 A. A. Ensafi, M. Jafari-Asl, N. Dorostkar, M. Ghiaci, M. Victoria Martínez-Huerta and J. L. G. Fierro, *J. Mater. Chem. B*, 2014, **2**, 706.
15 Y. Li, Y. Zhong, Y. Zhang, W. Weng and S. Li, *Sens. Actuators, B*, 2015, **206**, 735.
16 Y. Wang and F. Caruso, *Chem. Commun.*, 2004, 1528.
17 K. E. Toghill and R. G. Compton, *Int. J. Electrochem. Sci.*, 2010, **5**, 1246.
18 S. Park, H. Boo and T. D. Chung, *Anal. Chim. Acta*, 2006, **556**, 46.
19 P. Yang, X. Tong, G. Wang, Z. Gao, X. Guoand and Y. Qin, *ACS Appl. Mater. Interfaces*, 2015, **7**, 4772.
20 P. Si, X. C. Dong, P. Chen and D. H. Kim, *J. Mater. Chem. B*, 2013, **1**, 110.
21 Y. Li, Y. Zhonga, Y. Zhanga, W. Wenga and S. Li, *Sens. Actuators, B*, 2015, **206**, 735.
22 K. K. Lee, P. Y. Loh, C. H. Sow and W. S. Chin, *Biosens. Bioelectron.*, 2013, **39**, 255.
23 L. Ozcan, Y. Sahin and H. Turk, *Biosens. Bioelectron.*, 2008, **24**, 512–517.
24 M. Y. Elahi, H. Heli, S. Z. Bathaie and M. F. Mousavi, *J. Solid State Electrochem.*, 2007, **11**, 273.
25 M. D. S. M. Quintino, H. Winnischofer, M. Nakamura, K. Araki, H. E. Toma and L. Angnes, *Anal. Chim. Acta*, 2005, **539**, 215.
26 G. Sivasankari, C. Priya and S. S. Narayanan, *Int. J. Pharma Bio Sci.*, 2012, **2**, 188.

27 C. S. Shen, Y. Z. Wen, Z. L. Shen, J. Wu and W. P. Liu, *J. Hazard. Mater.*, 2011, **193**, 209.
28 M. d. S. M. Quintino, H. Winnischofer, K. Araki, H. E. Toma and L. Angnes, *Analyst*, 2005, **130**, 221.
29 X. Zeng, X. Liu, B. Kong, Y. Wang and W. Wei, *Sens. Actuators, B*, 2008, **133**, 381.
30 D. C. Crans, J. J. Smee, E. Gaidamauskas and L. Yang, *Chem. Rev.*, 2004, **104**, 849.
31 C. C. Lee, y. L. Hu and M. W. Ribbe, *Proc. Natl. Acad. Sci. U. S. A.*, 2009, **106**, 9209; R. Wever and M. A. Van der Horst, *Dalton Trans.*, 2013, **42**, 11778.
32 A. Bulter, *Coord. Chem. Rev.*, 1999, **187**, 17.
33 A. G. J. Ligtenbarg, R. Hage and B. L. Feringa, *Coord. Chem. Rev.*, 2003, **237**, 89.
34 D. Talukdar, K. Sharma, S. K. Bharadwaj and A. Thakur, *Synlett*, 2013, **24**, 963.
35 L. Rout and T. Punniyamurthy, *Adv. Synth. Catal.*, 2005, **347**, 1958.
36 S. Raghavan, A. Rajender, S. C. Joseph and M. A. Rasheed, *Synth. Commun.*, 2001, **31**, 1477.
37 M. Aschi, M. Crucianelli, A. D. Giuseppe, C. D. Nicola and F. Marchetti, *Catal. Today*, 2012, **192**, 56.
38 T. Itoh, K. Jitsukawa, K. Kaneda and S. Teranishi, *J. Am. Chem. Soc.*, 1979, **101**, 159.
39 C.-Y. Chu, D.-R. Hwang, S.-K. Wang and B.-J. Uang, *Tamkang J., Sci. Eng.*, 2003, **6**, 65.
40 K. H. Thomson, J. Lichter, C. LeBel, M. C. Scaife, J. H. McNeill and C. Orvig, *J. Inorg. Biochem.*, 2009, **103**, 554.
41 M. W. Makinen and M. Salehitazangi, *Coord. Chem. Rev.*, 2014, **279**, 1.
42 S. Kadota, I. G. Fantus, G. Deragon, H. J. Guyda and B. I. Posner, *J. Biol. Chem.*, 1987, **262**, 8252.
43 M. W. Makinen and M. J. Brady, *J. Biol. Chem.*, 2002, **277**, 12215.
44 J. F. Smalley, K. Chalfant, S. W. Feldberg, T. M. Nahir and E. F. Bowden, *J. Phys. Chem. B*, 1999, **103**, 1676.
45 H. O. Finklea, S. Avery, M. Lynch and J. Furtsch, *Langmuir*, 1987, **3**, 409.
46 K. Barman and S. Jasimuddin, *Catal. Sci. Technol.*, 2015, **5**, 5100.
47 L. Zhang and S. Dong, *J. Electroanal. Chem.*, 2004, **568**, 189.
48 A. J. Bard and L. R. Faulkner, *Electrochemical Methods: Fundamental and Applications*, John Wiley & Sons Inc., New York, 2001.
49 J. G. Velasco, *Electroanalysis*, 1997, **9**, 880.
50 E. Laviron, *J. Electroanal. Chem.*, 1974, **52**, 355.

Indian Journal of Chemistry
Vol. 53A, January 2014, pp. 57-61

Electrocatalytic oxidation of ascorbic acid by immobilized silver nanoparticles on self-assembled L-cysteine monolayer modified gold electrode

Koushik Barman & Sk Jasimuddin*

Department of Chemistry, Assam University
Silchar 788 011, Assam, India

Email: j.seikh@gmail.com

Received 23 April 2013; revised and accepted 26 December 2013

The electrocatalytic oxidation of ascorbic acid in phosphate buffer solution (*p*H 7.0) by immobilized silver nanoparticles (Ag@CTAB) on L-cysteine modified gold electrode is reported. The modified electrode has been characterized electrochemically using redox couple $[Fe(CN)_6]^{3-/4-}$. The electrocatalytic activity of the prepared electrodes is studied using cyclic voltammetry and electrochemical impedance spectroscopy. Electrochemical measurements show that the modified electrode (Au/L-cysteine/AgNPs) is highly active towards ascorbic acid oxidation. The oxidation peak of ascorbic acid at the Au/L-cysteine/AgNPs electrode is highly stable upon repeated potential cycling. The oxidation current of ascorbic acid increases upon each increment (0.05–0.35 μ*M*) in differential pulse voltammetry experiments. The oxidation current shows a linear relationship with the concentration of ascorbic acid with a correlation coefficient of 0.996. The detection limit of ascorbic acid was found to be 2×10^{-12} *M*. Common physiological interferents such as glucose, tartaric acid, citric acid and cysteine do not show any interference within the detection limit of ascorbic acid. The silver nanoparticles modified gold electrode has been used to determine the amount of ascorbic acid present in fruit and vegetable juices.

Keywords: Electrocatalytic oxidation, Ascorbic acid, Silver nanoparticles, L-Cysteine, Self-assembled monolayer, Gold electrode

Ascorbic acid (AA), the most ubiquitous vitamin present naturally in fruits and vegetables, is important in forming the protein collagen, and plays a paramount role as an antioxidant and preservative. Ascorbic acid has been widely used in food industry, pharmaceutical formulation and cosmetic applications. Therefore, an accurate, reliable and rapid method is needed for accurate determination of ascorbic acid. Different methods can be used for the quantitative estimation of AA such as volumetric titration[1,2], spectrophotometry[3,4], fluorimetry[5,6], high performance liquid chromatography[7,8], flow analysis[9,10], terbidimetry[11], etc. The detection of AA by voltammetric methods has received much attention in recent years[12]. Using a conventional electrode it is very difficult to determine AA accurately due to its high over-potential, poor reproducibility, low selectivity and sensitivity. Therefore, different approaches have been used to modify the electrode surface such as ion-exchange polymer[13], inorganic and organic materials[14,15] and self-assembled monolayers terminated with different functional groups[16].

Recently, modification of electrode surface with noble metal nanoparticles has received much attention mainly due to their interesting electrocatalytic and biosensing applications[17-23]. Detection of ascorbic acid using gold nanoparticles attached to glassy carbon (GC) electrode modified with 4-aminobenzoic acid followed by coupling with 4-aminothiophenol has been reported with the detection limit of 2.8 μ*M* AA[24]. The detection limit of 0.1 m*M* AA was reported at multilayers of AuNPs/redox polymers immobilized on GC electrode[25]. Electrocatalytic oxidation of AA by the immobilised citrate capped AuNPs on 1,6-hexanedithiol (HDT) modified Au electrode[26] has also been reported with a detection limit of of 1 μ*M* for AA.

Amongst all metal nanoparticles, silver nanoparticles (AgNPs) are of high interest because of their catalytic properties[27]. Traditionally, AgNPs have been employed as catalyst in different reactions. Also, Ag exhibits the highest electrical and thermal conductivity among all metals[28-30]. Herein, we present the electrocatalytic oxidation of AA in phosphate buffer solution by the positively charged silver nanoparticles (Ag@CTAB) immobilised on L-cysteine modified gold electrode (Au/L-cysteine/AgNPs) using cyclic voltammetry. The detection limit was calculated from differential pulse voltammetric studies and to the best of our knowledge is lowest detection limit reported for ascorbic acid using metal nanoparticles. The Au/L-cysteine/AgNPs modified electrode is very stable and provides a very sensitive, selective, reliable, easy to perform and fast method for AA determination. The present modified electrode has been applied for the determination of AA present in fruit and vegetable juices.

Experimental

L-cysteine (Sisco Research Laboratories) and $AgNO_3$ (Qualigen Fine Chemicals) were used as received. Sodium borohydride and ascorbic acid were purchased from SD Fine Chemicals Ltd., while cetyltrimethyl ammonium bromide (CTAB) was obtained from Central Drug House (P) Ltd. All other chemicals were of analytical grade and used without further purification. Phosphate buffer saline (PBS) solution was prepared by mixing 0.1 *M* $NaClO_4$ and 0.01 *M* H_3PO_4 using Smalley method[31]. The *p*H of the solution was adjusted with 0.11 *M* NaOH. The Au electrode was polished using aqueous slurries of gamma alumina oxide (0.05 micron) and sonicated in doubly distilled water. The mechanically polished Au electrode was then cleaned electrochemically by cycling the potential between –0.2 V and 1.6 V versus Ag/AgCl reference electrode in 1 *M* H_2SO_4 at a scan rate 100 mV/s until the characteristic reproducible voltammograms were obtained.

Electrochemical measurements were performed with a conventional three-electrode cell with a gold electrode as working electrode, a Pt wire as counter electrode and Ag/AgCl (0.03 *M* KCl) as reference electrode. All electrochemical experiments were carried out with CH Instrument-660C electrochemical workstation. UV-vis spectra were recorded on a Shimadzu UV-3101PC spectrophotometer.

CTAB capped Ag nanoparticles (Ag@CTAB) were prepared by adding 2 mL of ice cold solution of 0.1 *M* $NaBH_4$ to 1.25 mL of 10^{-2} *M* $AgNO_3$ prepared in 48.75 mL of 0.01 *M* CTAB solution under vigorous stirring for eight hours. The colourless solution changed slowly to yellow, indicating the formation of AgNPs[32]. The solution was stored at 4 ^oC in a dark bottle until further use. Characteristic UV-vis absorption of the CTAB capped Ag nanoparticles, with the sharp peak appearing at 410 nm was observed (Supplementary data, Fig. S1).

The electrochemically cleaned electrode was immersed in 10 m*M* L-cysteine solution containing 0.1 *M* $HClO_4$ for 24 h to allow the chemisorptions of the reagent on to the gold. The modified gold was then rinsed thoroughly with ethanol and water. Immobilisation of Ag nanoparticles on Au/L-cysteine modified SAM electrode was done by dipping the Au/L-cysteine electrode into an Ag colloidal solution for 4 h. The resultant electrode was washed with doubly distilled water and used for electrochemical measurements of AA.

Results and discussion

Figure 1 shows the cyclic voltamograms of 0.5 m*M* $[Fe(CN)_6]^{3-/4-}$ obtained for bare Au, Au/L-cysteine and Au/L-cysteine/AgNPs electrodes in PBS at *p*H 7. The bare Au electrode exhibits a quasi-reversible voltammetric response for $[Fe(CN)_6]^{3-/4-}$ redox couple with a peak separation of 116 mV (curve 1) at a scan rate of 100 mV/s. The cathodic peak current was significantly decreased (2.4×10^{-6} A to 8.6×10^{-7} A) in the case of Au/L-cysteine SAM modified electrode as compared to bare Au electrode. This suggests that the monolayer of L-cysteine was densely packed on Au electrode surface and thus effectively blocked the electronic communication between the $[Fe(CN)_6]^{3-/4-}$ in solution and the underlying gold electrode surface. After the immobilisation of AgNPs on Au/L-cysteine electrode the cathodic current peak increased from 8.6×10^{-7} A to 3.5×10^{-6} A with a peak separation of 67 mV (curve 3), indicating that the Ag nanoparticles were successfully immobilized on the L-cysteine modified gold electrode and a good electronic communication was achieved between the redox species $[Fe(CN)_6]^{3-/4-}$ in solution and the underlying Au electrode through AgNPs.

The influence of *p*H of electrolyte solution on the electrochemistry of immobilized AgNPs over Au-L-cysteine SAM was studied. The cathodic peak current reached the maximum value at *p*H 7.0. Beyond this *p*H, the cathodic peak current decreased. It is known that the isoelectric point of native cysteine is 5.06 and with a negative charge on cysteine in the

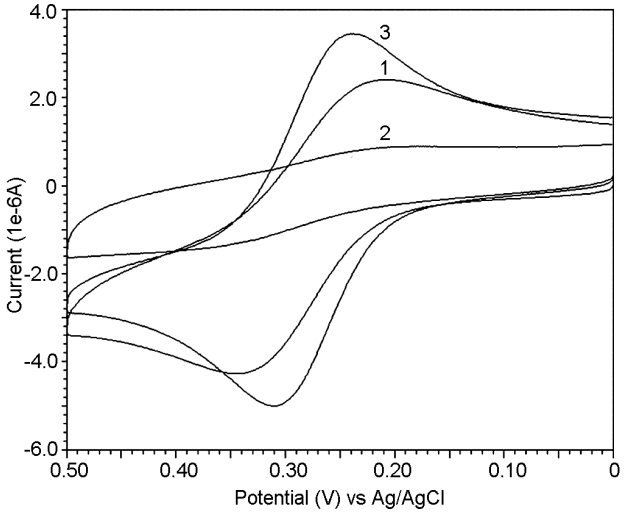

Fig. 1 — Cyclic voltammograms of 0.5 m*M* $K_4[Fe(CN)_6]$ at *p*H 7 using different working electrodes. [1, bare Au electrode; 2, modified Au/L-cysteine electrode; 3, modified Au/L-cysteine/ AgNPs electrode].

*p*H domain of 6.0–7.5. In other words, the L-cysteine coated gold electrode carries negative charge in this *p*H range. At *p*H 7.0, the interaction between positively charged Ag nanoparticles and the negatively charged L-cysteine reached a maximum as is observed from the cathodic peak current. At low *p*H, a poor response was obtained, as shown by low currents. This is due to poor interaction between the carboxyl group and the positively charged Ag nanoparticles. A representative cyclic voltamogram at varying *p*H (2.0 to 7.0) is given in Fig. S2 (Supplementary data). At the higher *p*H range (7.5–10.0), the free amino group may interact with the gold surface and weaken the interaction between amine group and AgNPs, showing low current height. At high *p*H (> 10.0) the signal was unstable and disappeared.

The cyclic voltammograms obtained in the presence of 0.5 m*M* ascorbic acid, 0.1 *M* PBS and at *p*H 7, on bare Au, Au/L-cysteine SAM electrode and Au/L-cysteine/AgNPs modified electrode are represented in Fig. 2. An irreversible oxidation of AA occured at 0.34 V at Au/L-cysteine/AgNPs modified electrode, which was 100 mV less positive than the oxidation of AA (0.44 V) at Au/L-cysteine electrode; the oxidation current of AA increased from 4.6 μA to 5.4 μA. This behaviour demonstrates electrocatalytic activity for Au/L-cysteine/AgNPs electrodes towards AA oxidation. No reduction peak appeared for ascorbic acid on bare or modified electrodes. This confirms the data reported in literature that electrochemical oxidation of ascorbic acid is an irreversible process[35].

Electrochemical impedance spectroscopy (EIS) was carried out in 0.5 *M* ascorbic acid at *p*H 7.0 (PBS buffer) using modified working electrodes (bare Au electrode, Au/L-cysteine SAM electrode and Au/L-cysteine/AgNPs modified electrode) where the frequency range was 0.01 Hz to 100000 Hz and E_{ac} = 10 mV. The diameter of the semicircle observed in the Nyquist plot corresponds to the charge transfer resistance, R_{ct}; the smaller the semi-circle, faster is the charge or electron transfer[33]. Figure 3 shows that the semi-circle decreases upon immobilisation of AgNPs on Au/L-cysteine SAM electrode surface. The decrease in semi-circle (R_{ct}) shows the following trend: bare Au (2.518×10^6 Ω) > Au/L-cysteine (13.776×10^3 Ω) > Au/L-cysteine/AgNPs (7.574×10^3 Ω). The observed trend is due to the fact that the modified electrodes facilitate electron transfer rate for the oxidation of ascorbic acid to dehydroascorbic acid. Impedance measurements clearly show that Au/L-cysteine/AgNPs exhibits lower resistance as compared to the bare Au and Au-L-cysteine SA modified electrodes. This study shows that the Au/L-cysteine/AgNPs modified electrode is an efficient electrocatalyst for AA oxidation.

The dependence of voltammetric response on the ascorbic acid concentrations at Au/L-cysteine/AgNPs

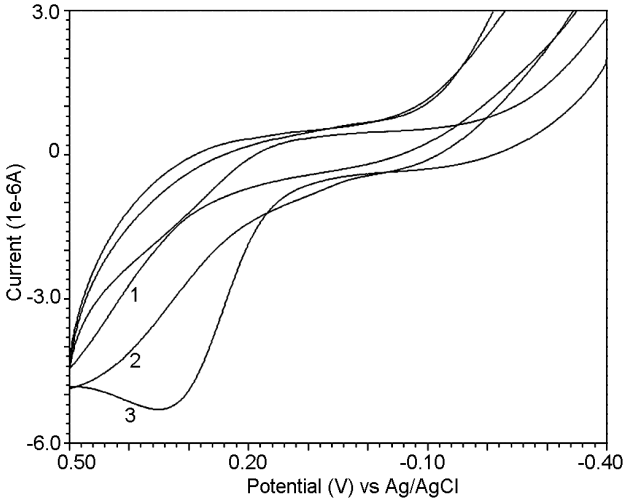

Fig. 2 — Cyclic voltammogram of 0.5 m*M* ascorbic acid in 0.1 *M* PBS solution at *p*H 7 using different working electrodes. [1, bare Au electrode; 2, modified Au/L-cysteine electrode; 3, modified Au/L-cysteine/AgNPs electrode].

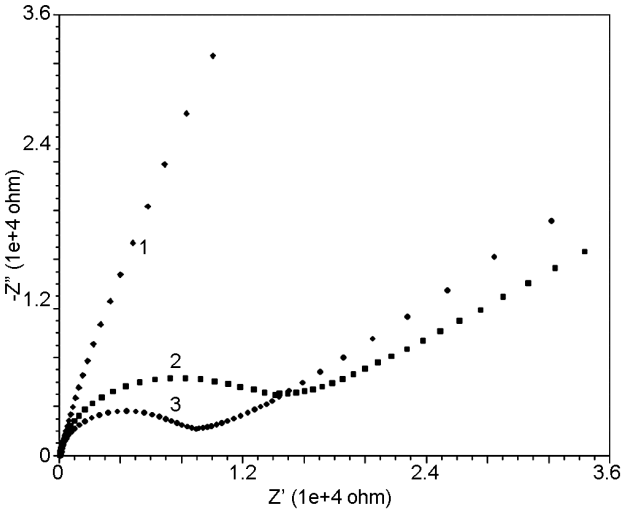

Fig. 3 — Nyquist plot ($-Z''$ versus Z') of 0.5 m*M* ascorbic acid in 0.1 *M* PBS solution at *p*H 7 using various working electrodes obtained from impedance measurements. [1, bare Au electrode; 2, modified Au/L-cysteine electrode; 3, modified Au/L-cysteine/AgNPs electrode].

Table 1— Determination of ascorbic acid content in various fruit and vegetable juices using DPV

Sample (juice)	Initial current (μA)	Current after addition of standard AA solution (μA)	AA acid conc. (mg/100 mL juice)	Ascorbic acid ($\times 10^{-3}$ *M*)		Recovery (%)
				Added	Found	
Orange	-0.6891	-0.8395	39.91	1	1.0585	105.85
Lemon	-0.8171	-0.9855	47.52	1	0.9996	99.96
Apple	-0.6566	-0.8335	34.41	1	0.9995	99.95
Grape	-0.6523	-0.8480	51.05	1	0.9991	99.91
Tomato	-0.6603	-0.7552	29.18	1	1.0003	100.03
Cabbage	-0.4534	-0.5227	18.59	1	0.9996	99.96
Cauliflower	-0.6538	-0.7922	26.00	1	0.9992	99.92

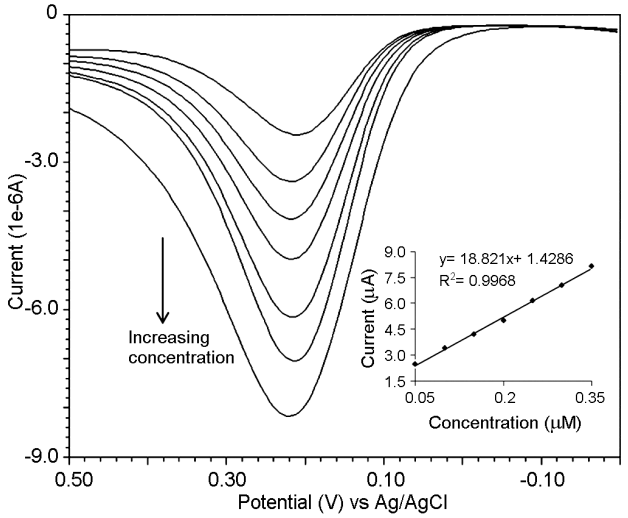

Fig. 4 — Overlaid DPV with increasing ascorbic acid concentration (0.05—0.35 μ*M*) in 0.1 *M* PBS (*p*H 7) at Au/L-cysteine/AgNPs modified electrode. [Inset: Plot of current as a function of concentration of ascorbic acid with linear trend line ($R^2 > 0.99$)].

modified electrode was studied using DPV. Figure 4 shows the DPV responses of the modified electrode towards AA at varying concentrations. The oxidation current of AA increases linearly in the range of 0.05–0.35 μ*M*, (linear regression equations: I_p (μA) = 18.821 *C* (μ*M*)+1.4286 with a correlation coefficient of 0.996, as shown in Fig. 4 (inset)). Detection limit of 2×10^{-12} *M* for AA was obtained using $3\sigma/m$, where σ is the standard deviation (1.259×10^{-11} A) of the peak current in blank solution, n = 25 and m (18.826 μA/μ*M*) is the slope of the calibration curve). The detection limit was further confirmed by chronoamperometry (Supplementary data, Fig. S3).

The application of Au/L-cysteine/AgNPs modified electrode for the determination of AA at 0.5 μ*M* concentration was also checked in the presence of 0.5 m*M* concentration of glucose, tartaric acid, citric acid, and cysteine as interferents in PBS solution (*p*H 7). In the presence of interferents, the oxidation peak potential of AA was stable and the current response of AA was also not affected (Supplementary data, Fig. S4). Thus, Au/L-cysteine/AgNPs modified electrode may be successfully used to determine the concentration of AA in the presence of physiologically common interferents.

Fruit (orange, lemon, apple, and grape) and vegetable (tomato, cabbage, and cauliflower) juices were obtained by pressing. The stock solution (1 mL juice was diluted with 9 mL PBS buffer solution; *p*H = 7) was prepared and DPV was recorded in each case with the Au/L-cysteine/AgNPs modified electrode. The ascorbic acid content was calculated by measuring the peak currents obtained for sample solutions and after addition of standard AA solution, using the equation $I = KC$, where I is the current obtained for sample solution and K is the increased amount of current after addition of standard AA solution and C is the unknown concentration. The obtained results are presented in Table 1 and agree with the data reported in literature[34-36]. The accuracy of the method was also verified by recovery studies adding standard ascorbic acid solutions to samples. Recoveries of 99.91–105.85% were achieved. A representative DPV for AA in orange juice solution and after addition of standard AA solution is shown in Fig. S5 (Supplementary data). Also, recovery and reproducibility of these measurements were satisfactory.

The present study demonstrates an excellent approach for the development of a novel silver nanoparticles/L-cysteine modified gold electrode for the electrocatalytic oxidation of ascorbic acid. Fast electron transfer and high stability for the oxidation of ascorbic acid were achieved at the Au/L-cystine/AgNPs modified electrode. The electrocatalytic oxidation of AA showed the following order of the studied electrode: Au/L-cysteine/AgNPs > Au/L-cysteine > bare Au. EIS results are consistent

with the CV responses. The DPV results indicate that the Au/L-cysteine/AgNPs modified electrode has a superior detection limit (2.0×10^{-12} *M*) than earlier reported gold nanoparticles modified electrode systems. This electrode selectively determines ascorbic acid in presence of physiologically common interferents and has been successfully used for analysis in fruit and vegetable juices with good recovery. The sensor displays good storage stability if kept in aqueous medium at room temperature. The Au/L-cysteine/AgNPs modified electrode retained its initial activity after one–two weeks of storage.

Supplementary data

Supplementary data associated with this article, i.e., Figs S1-S5, are available in the electronic form at http://www.niscair.res.in/jinfo/ijca/IJCA_53A(01)57-61_SupplData.pdf.

References

1 Lenghor N, Jakmunee J, Vilen M, Sara R, Christian G D & Grudpan K, *Talanta*, 58 (2002) 1139.
2 Rajantie H, Strutwolf J & Williams D E, *J Electroanal Chem,* 500 (2001) 108.
3 Serrano I O, Jover T H & Belloso O M, *Food Chem*, 105 (2007) 1151.
4 Chen H S O, Ng S C & Seow S H, *Synth Met*, 66 (1994) 177.
5 Arya S P, Mahajan M & Jain P, *Anal Chim Acta*, 417 (2000) 1.
6 Tetsuharu I, Shuuji H, Masatoshi Y, Masaru N & Yosuke O, *Chem Pharm Bull,* 33 (1985) 3499.
7 7 Shekhovtsova T N, Muginova S V, Luchinina J A & Galimova A Z, *Anal Chim Acta*, 573-574 (2006) 125.
8 Lykkesfeldt J, *Anal Biochem,* 282 (2000) 89.
9 Paim A P S, Almeida C M N V, Reis B F, Lapa R A S, Zagotto E A G & Lima J L F C, *J Pharm Biomed Anal,* 28 (2002) 1221
10 Prez-Ruiz T, Martinez-Lozano C, Sanz A & Guillen A, *J Pharm Biomed Anal*, 34 (2004) 551.
11 Spickenreither M, Braun S, Bernhardt G, Dove S & Buschauer A, *Bioorg Med Chem Lett,* 16 (2006) 5313.
12 Martin Jr D W in *Harper's Review of Biochemistry*, edited by D W Martin Jr, P A Mayes & V W Rodwell, 19th Edn, (Lange Los Altos, CA) 1983.
13 Zen J M, Chen Y J, Hsu C T & Ting Y S, *Electroanalysis*, 9 (1997) 1009.
14 Freire R S & Kubota L T, *Analyst*, 127 (2002) 1502.
15 Raj C R & Ohsaka T, *J Electroanal Chem*, 540 (2003) 69.
16 Raj C R, Tokuda K & Ohsaka T, *Bioelectrochem*, 53 (2001) 183.
17 Rad A S, Mirabi A, Binaian E & Tayebi H, *Int J Electrochem Sci*, 6 (2011) 3671.
18 Chao M & X Ma, *Int J Electrochem Sci*, 7 (2012) 6331.
19 Wang L, Zhu H, Hou H, Zhang Z, Xiao X & Song Y, *J Solid State Electrochem*, 16 (2012) 1693.
20 Murray R W, *Chem Rev*, 108 (2008) 2688.
21 Nam E J, Kim E J, Wark A W, Rho S, Kim H & Lee H J, *Analyst*, 137 (2012) 2011.
22 Campas M, Garibo D & Simon B P, *Analyst,* 137 (2012) 1055.
23 Sanghavi B J, Mobin S M, Mathur P, Lahiri G K & Srivastava A K, *Biosensors Bioelectronics*, 39 (2013) 124.
24 Zhang L & Jiang X, *J. Electroanal Chem*, 583 (2005) 292.
25 Qian L, Gao Q, Song Y, Li Z & Yang X, *Sensor Actuat B*, 107 (2005) 303.
26 Sivanesan A, Kannan P & John S A, *Electrochim Acta*, 52 (2007) 8118.
27 Sun Y G & Xia Y N, *Science,* 298 (2002) 2176.
28 Verykios X E, Stein F P & Coughlin R W, *Catal Rev-Sci Eng*, 22 (1980) 197.
29 Sun T & Seff K, *Chem Rev*, 94 (1994) 857.
30 Russell A & Lee K L, *Structure-Property Relations in Nonferrous Metals*, (John Wiley & Sons) 2005, p 322.
31 Smalley J F, Chalfant K, Feldberg S W, Nahir T M & Bowden E F, *J Phys Chem B*, 103 (1999) 1676.
32 Wang W & Gu B, in *Concentrated Dispersions: Theory, Experiment and Applications*, edited by P Somasundaran & B Markovic, *ACS Symposium Series 878*, (Oxford University Press) 2004, Chap. 1, p. 1.
33 Mashazi P N, Westbroek P, Ozoemena K I & Nyokong T, *Electrochim Acta*, 53 (2007) 1858.
34 Matsumoto K, Yamada K & Osajima Y, *Anal Chem*, 53 (1981) 1974.
35 Pisoschi A M, Danet A F & Kalinowski S, *J Automat Meth Manag Chem,* 2008 (2008) 937651 and references therein.
36 Pisoschi A M, Pop A, Negulescu G P & Pisoschi A, *Molecules*, 16 (2011) 1349.

RSC Advances

COMMUNICATION

Cite this: *RSC Adv.*, 2016, **6**, 99983

Received 5th August 2016
Accepted 8th October 2016

DOI: 10.1039/c6ra19813a

www.rsc.org/advances

Simultaneous electrochemical detection of dopamine and epinephrine in the presence of ascorbic acid and uric acid using a AgNPs–penicillamine–Au electrode†

Koushik Barman and Sk. Jasimuddin*

A highly selective and sensitive electrochemical sensor, AgNPs–penicillamine–Au, was developed for the simultaneous detection of dopamine (DA) and epinephrine (EP) in the presence of a high concentration of ascorbic acid (AA) and uric acid (UA). Microscopy and voltammetry techniques were used for the characterization of the modified electrode. Chronoamperometry was used for the determination of DA and EP in the linear range of 0.1 to 100.0 μM with detection limits of 0.2 nM and 0.5 nM, respectively. The simultaneous determination of DA, EP, AA and UA was achieved by using differential pulse voltammetry. The proposed sensor was successfully applied for the simultaneous determination of DA and EP in human blood sample with excellent recovery.

Introduction

Dopamine (DA) and epinephrine (EP) are two important catecholamine neurotransmitters that communicate information throughout our brain and body. The brain uses these neurotransmitters to stimulate the heart to beat, the lungs to breathe, and the stomach to digest food.[1] Low levels or complete depletion of DA and EP in the central nervous system is implicated as a major cause of several neurological disorders like Parkinson's disease, Schizophrenia, Huntington's disease, as well as drug addiction and HIV.[2] Medically DA and EP are very common emergency health care medicine and have been used in hypertension, bronchial asthma, cardiac surgery, myocardial infection *etc.*[3] Thus it is necessary to develop quantitative methods for their sensitive and selective determination in a simultaneous way. Different methods are used to determine DA and EP simultaneously, including high performance liquid chromatography-mass spectroscopy,[4] capillary electrophoresis,[5] chemiluminescence,[6] flow injection analysis,[7] spectrophotometry[8] and electrochemical methods.[9] Due to simple procedures, high sensitivity, reproducibility, economic and ease of miniaturization electrochemical sensor were explored to determine DA and EP. Dopamine and epinephrine are often coexisting with ascorbic acid (AA) and uric acid (UA) in biological sample. In the electroanalytical methods at most solid electrodes, they can all be oxidized at similar potential resulting in an overlapping voltammetric response. Therefore, the simultaneous electrochemical detection of DA and EP in the presence of AA and UA is a real challenge in the field of pathological and drug development research. For their simultaneously detection many different strategies have been employed for the modification of electrode surface but only few electrochemical sensor has been exploited which can able to detect simultaneously DA, EP, AA and UA.[10] Among different modification process self-assembled monolayer (SAMs) of organosulphur compounds on metal surfaces comprise a wide range of potential applications due to their versatility in modifying surfaces in a controllable manner. It has been shown that organothiol molecules adsorb at gold *via* S–Au bond formation using oxidative addition and reductive elimination process.[11] Penicillamine, $(CH_3)_2C(SH)CH(NH_2)$-(COOH), can form highly stable self-assembled gold electrode and used for the study of electrochemical behaviour of DA and EP in an individual basis.[12,13] The main drawback of such modified electrode is that they cannot detect DA and EP simultaneously because they oxidized at similar potential at penicillamine–Au electrode. To overcome such limitation of penicillamine modified electrode, we introduce silver nanoparticles over penicillamine self-assembled gold electrode. Among different metal nanoparticles, silver nanoparticles are of special interest due to their catalytic properties.[14] Traditionally, AgNPs have been used as catalyst in various reactions. Beside this silver exhibits the highest electrical conductivity among all metals.[15] In the present communication we first time reported that AgNPs–penicillamine–Au electrode can detect DA and EP simultaneously in the presence of high concentration of AA and UA at neutral pH. A well separated oxidation peaks for DA, EP, AA and UA was observed at the AgNPs–penicillamine–Au electrode in phosphate buffer solution (pH 7.0). Diffusion

Department of Chemistry, Assam University, Silchar, Assam-788011, India. E-mail: sk.jasimuddin@aus.ac.in

† Electronic supplementary information (ESI) available: Figures, tables, references *etc.* See DOI: 10.1039/c6ra19813a

coefficient, electron transfer coefficient and the catalytic reaction rate were also examined for DA and EP. The proposed modified gold electrode has been applied to the simultaneous voltammetric measurement of DA, EP and AA, UA in human blood sample with satisfactory results.

Experimental

Chemicals and reagents

Dopamine, epinephrine, penicillamine (PCA), ascorbic acid (AA), uric acid (UA), $AgNO_3$, polyvinylpyrilidone (PVP) were purchased from Sigma Aldrich, India, $K_4[Fe(CN)_6]_3 \cdot H_2O$ were purchased from Merck (India). Human whole blood was obtained from Barak blood bank, Silchar, Assam. All the reagents and solvents were analytical grade and were used without further purification. Phosphate buffer solution (0.1 M) was prepared by mixing 0.1 M $NaClO_4$ and 0.01 M H_3PO_4 and the pH's were adjusted by the addition of 0.11 M NaOH using Smalley's method.[16] Double distilled water was used throughout the course of the experiment.

Apparatus and instrumentations

All electrochemical measurements were performed with a CHI 660C Electrochemical workstation (CH Instrument, USA). A conventional three electrode system was employed, which consisted with a gold or modified gold electrode as working electrode (2 mm diameter, 0.031 cm^2 area), Pt wire as a counter electrode and Ag/AgCl (3 M KCl) as reference electrode. All experiments were performed at ambient temperature and inert atmosphere. High resolution transmission electron microscopy (HR-TEM) images were obtained using JEM-100CX, Jeol. UV-vis spectra were recorded on a Shimadzu UV-3101PC spectrophotometer. pH measurement of solutions was carried out on a pH meter (Macro Scientific Works (Regd), New Delhi).

Synthesis of silver nanoparticles

In an ethanolic solution of 0.001 M silver nitrate and 0.5% PVP, 0.1 M ascorbic acid was added drop wise and stirred for half an hour under nitrogen atmosphere. The colourless solution slowly changed into a yellowish brown indicating the formation of silver nanoparticles. By varying the added percentage of PVP, different sized AgNPs were prepared. After preparing, the AgNPs solution was kept in a sample tube for further use.

Construction of AgNPs–penicillamine modified gold electrode

A gold electrode was polished with wet α-alumina (0.5 μm) on a flat polishing pad for 10 minutes and rinsed several times with doubly distilled water. The cleanliness of the gold electrode surface was ascertained by recording the repetitive cyclic voltammograms in 0.5 M H_2SO_4 between −0.2 and +1.5 V *versus* Ag/AgCl with 0.1 V s^{-1} scan rate until a steady characteristic gold oxide cyclic voltammogram was obtained.[17] The electrode was then rinsed with doubly distilled water and immersed in 1.0 mM ethanolic solution of penicillamine (PCA) for 24 hours. The PCA was self-assembled over the gold electrode surface *via* gold–sulphur interaction and the modified electrode PCA–Au was thoroughly washed with double distilled water. Thereafter, the PCA modified gold electrode was dipped into AgNPs solution for 4 hours under stirring condition and AgNPs–PCA modified gold electrode (AgNPs–PCA–Au) was formed. The finally modified electrode was washed thoroughly with distilled water and dried in air for further use.

Results and discussion

Characterization of AgNPs

HR-TEM. To investigate morphological features of the prepared AgNPs, TEM image was recorded and is shown in Fig. 1a. The corresponding particle size distribution histogram is given in Fig. 1b which shows that the diameter of the nanoparticles is around 4 nm. Fig. 1c shows the lattice fringes (0.141 nm) on the surface, which is in good agreement with the interplaner spacing of Ag (220). The nanocrystalline nature of AgNPs was evidenced by the selected area electron diffraction (SAED) pattern. Fig. 1d with bright circular spots corresponding to (111), (200), (220) and (311) characteristic of the face centred cubic Ag (JCPDS card no. 89-3722).

UV-vis spectroscopy. UV-visible spectra of AgNPs@PVP in ethanol (Fig. S1†) shows a single and sharp surface resonance resonance peak at 390 nm (ref. 18) and support the formation of nearly spherical silver nanoparticles.

Cyclic voltammetry. The electrochemical behaviour of AgNPs was studied using cyclic voltammetry. Fig. S2† illustrate the cyclic voltammograms obtained at bare, PCA and AgNPs–PCA modified gold electrode in 0.1 M PBS (pH 7.0). A sharp irreversible oxidation peak was observed at +0.215 V *versus* Ag/AgCl at AgNPs–PCP–Au electrode whereas no such characteristic peak was observed for bare-Au and PCA–Au electrode in the same potential region. This observation reveals that the AgNPs over PCA–Au electrode are more prone to oxidation as compared to reduction, which can be attributed to the reaction $Ag^{\circ} \rightarrow Ag^{+} + e^{-}$. Fig. S3a† shows that with increasing scan rate, the oxidation peak of AgNPs was enhanced and at the same time the peak potential was slightly shifted positively with increasing scan rate. The linear variation of peak current with scan rate

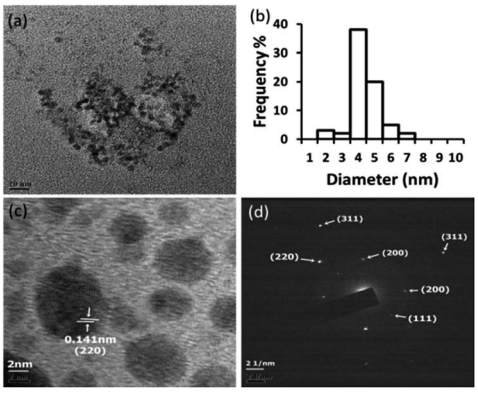

Fig. 1 TEM images of AgNPs (scale bar 20 nm) (a), particle size distribution histogram of AgNPS (b), HRTEM image showing lattice fringes (c), and a typical SAED of AgNPs (d).

(Fig. S3b†) indicates surface confined process involved in the electrode reaction due to the formation of thin layer of AgNPs over PCA–Au.

Characterization of modified electrode

FE-SEM. The stepwise modification of pure gold electrode surface was characterized by FE-SEM (Fig. S4†). Fig. S4a† shows a smooth surface morphology for bare gold electrode and remains almost smooth after modification with PCA (Fig. S4b†) suggesting well ordered and densely packed layer formation over gold surface. After immobilization of AgNPs over the PCA–Au, no characteristic change of the surface morphology was observed (Fig. S4c†) and this may be due to very small particle size (4 nm) of AgNPs. Elemental mapping images show the presence of O, S and Ag which confirms the formation of AgNPs–PCA–Au electrode (Fig. S4d†).

Electrochemical characterization

The characterization of AgNPs–PCA–Au electrode was conducted using the reversible redox couple $[Fe(CN)_6]^{3-}/[Fe(CN)_6]^{4-}$. Fig. S5† shows the overlapped cyclic voltammograms of 0.5 mM $[Fe(CN)_6]^{4-}$ in 0.1 M phosphate buffer solution (pH = 7.0) at bare Au, PCA–Au and AgNPs–PCA–Au electrode. A quasireversible redox couple was observed at bare gold electrode and after modification with PCA the oxidation peak was shifted in the positive potential region with decreased in current height which supports the formation of self-assembled monolayer of PCA over Au electrode. After AgNPs immobilization over PCA–Au electrode, a quasireversible $[Fe(CN)_6]^{4-}/[Fe(CN)_6]^{3-}$ couple (ΔE = 70 mV) was obtained with large increase of peak current height. This is due to the better electronic communication between the redox probe and the gold electrode through AgNPs. Electrochemical impedance spectroscopy (EIS) supports the CV results. In the Nyquist plot (Fig. S6†), the diameter of the semicircle (R_{CT}) was increased from 1.0×10^5 (bare Au) to 5.0×10^5 Ω (PCA–Au) indicates that the PCA modified Au electrode was blocked the electron transfer between gold electrode and redox probe. After immobilizing AgNPs on the PCA–Au electrode, the R_{CT} values decrease to 0.1×10^5 Ω suggesting low resistance and hence much more electron transfer between the probe and gold electrode through AgNPs. The results also support the proper modification of gold electrode.

Electrochemical studies of dopamine and epinephrine at AgNPs–PCA–Au electrode

Electrocatalytic oxidation of DA and EP were studied using cyclic voltammetry and electrochemical impedance spectroscopy. Cyclic voltammogram of 10 μM DA was recorded in 0.1 M PBS at the bare Au, PCA–Au and AgNPs–PCA–Au with a scan rate of 100 mV s^{-1} (Fig. 2a). An irreversible redox couple ($\Delta E = E_{pa} - E_{pc}$ = 0.28 V) with the anodic peak potential (E_{pa}) at +0.50 V is observed at the bare gold electrode. At PCA modified gold electrode, the E_{pa} value is shifted to +0.25 V with increase of current height (I_{pa} = 2.0 μA). Using AgNPs–PCA–Au electrode, a distinct redox couple for DA is observed with large increase of current height (I_{pa} = 15.0 μA) and more negative

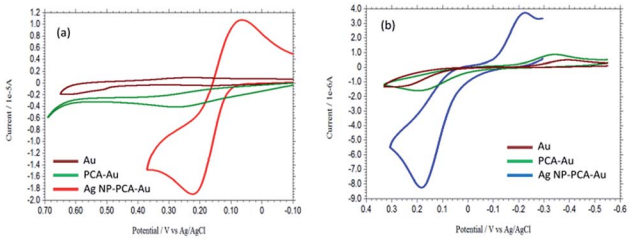

Fig. 2 Cyclic voltammogram of 10 μM DA (a) and 10 μM EP (b) in 0.1 M PBS (pH 7.0) at bare, PCA and AgNPs–PCA modified gold electrodes.

shifting of the anodic peak potential (+0.22 V). Similarly, for EP the oxidation peak potential is shifted to the less positive potential with large increase of current height when bare, PCA modified and AgNPs–PCA modified gold electrodes is used successively (Fig. 2b). These observations support the electrocatalytic nature of AgNPs–PCA–Au electrode for the oxidation of DA and EP. In the EIS experiment, the diameter of the semicircle obtained from the Nyquist plot ($-Z''$ *versus* Z') correspond to the charge transfer resistance (R_{CT}); the smaller the diameter of semicircle, faster is the charge transfer and *vice versa*.[19] Fig. S7 and S8† shows that the diameter of the semi-circle decreases upon modification of gold electrode surface. The R_{CT} values in different electrode system shows the following trend: bare Au (2.0×10^4 Ω) > PCA–Au (1.0×10^4 Ω) > AgNPs–PCA–Au (0.2×10^4 Ω) and bare Au (5.0×10^4 Ω) > PCA–Au (3.0×10^4 Ω) > AgNPs–PCA–Au (0.8×10^4 Ω) for DA and EP, respectively. The observed trend suggests that the maximum electron transfer between gold surface and the analyte DA or EP is occurred at AgNPs–PCA–Au electrode. This study also indicates that the AgNPs modified PCA–Au electrode is an efficient electrocatalyst for the oxidation of DA and EP under neutral pH.

To study the size dependent electrochemical sensing behaviour of the AgNPs for DA and EP, three different sizes of AgNPs (*viz.*, 4, 10 and 20 nm, by varying the PVP amount as 0.5, 0.3 and 0.1%, respectively) were employed. The cyclic voltammogram (Fig. S9a and c†) shows that the oxidation of DA and EP occurred at low positive potential with large current height at 4 nm sized AgNPs immobilized PCA–Au electrode compared to the 10 or 20 nm AgNPs modified electrode. This observation inferred that the 4 nm size AgNPs have higher electrocatalytic activity (higher sensing) than the larger size AgNPs. EIS (Fig. S9b and d†) and chronoamperometry (Fig. S10a and b†) data also supports the higher electrocatalytic sensing ability of AgNPs (4 nm)–PCA–Au electrode. By considering the size dependency results, ~4 nm sized AgNPs immobilized PCA–gold electrode is used in the subsequent experiments.

Determination of dopamine and epinephrine using chronoamperometry and DPV

Determination of DA and EP were performed under optimized condition using chronoamperometry. Fig. S11 and S12† shows the chronoamperograms at the fixed potential +0.22 V and +0.18 V (*versus* Ag/AgCl) with increasing concentration of DA

and EP in 0.1 M PBS using AgNPs–PCA–Au as working electrode, respectively. The current *versus* concentration plots for DA and EP were linear with their concentration in the range of 0.1 to 100 μM at 30 seconds. The linear regression equation were $I = 2.9124C + 5.6602$ ($R^2 = 0.9997$), with a detection limit of 0.20 nM (S/N = 3) and $I = 1.5465C + 2.4035$ ($R^2 = 0.9996$), with a detection limit of 0.51 nM (S/N = 3) for DA and EP, respectively. Differential pulse voltammetry was used for further confirmation of the detection limit and the result was satisfactory (Fig. S13 and S14†). Simultaneous determination of DA and EP were performed using DPV. Fig. S15† shows the DPV curves of DA with different concentrations in the presence of 0.2 μM EP and the reductive peak current of DA was linear with its concentration range of 0.2 to 1.0 μM. The regression equation was $I_{pc} = 2.91C + 4.93$ ($R^2 = 0.9905$) with a detection limit of 0.20 nM (S/N = 3). Similarly, Fig. S16† shows the DPV curves for different concentration of EP in the presence of fixed concentration (0.2 μM of DA) and the reduction peak current of EP increased linearly in the concentration range of 0.2 to 1.0 μM. The regression equation was $I_{pc} = 1.347C + 3.0542$ ($R^2 = 0.9977$) with a detection limit of 0.51 nM (S/N = 3). For further evaluating the feasibility of the simultaneous determination of DA and EP at AgNPs–PCA–Au electrode, DPV was taken by changing their concentration simultaneously (Fig. 3). All the results support the simultaneous and sensitive detection of DA and EP at AgNPs–PCA–Au electrode. Fig. 4 shows the DPV of DA and EP in presence of 1000 times higher concentrations of UA and AA and the results supports the selective determination of DA and EP is possible in presence of large excess of UA and AA. Fig. S17 and S18† illustrates the DPV responses of the proposed electrode towards EP, DA, AA and UA when the concentrations of the four species increase simultaneously. It can be seen that both the reduction and oxidation peak current for all four species increases linearly with their concentrations. The DPV responses of the AgNPs–PCA–Au electrode towards the simultaneous determination of these four analytes are listed in Table S1.† The RSD of the peak current was less than 2.5% for these four species at AgNPs modified gold electrode ($n = 10$). In comparison to other electrochemical sensors, the proposed AgNPs–PCA–Au electrode exhibited improved analytical performance as shown in Table S2.†

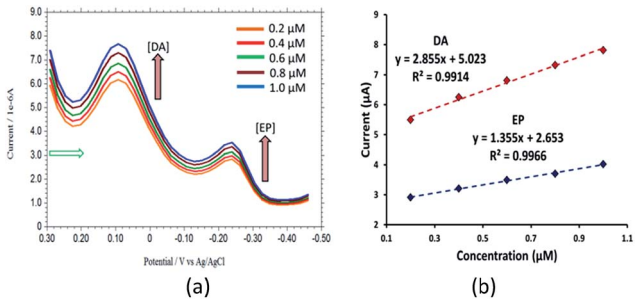

Fig. 3 Overlaid DPV for simultaneous increase of concentration of DA and EP in 0.1 M PBS at AgNPs–PCA–Au electrode (a). Plot of current as a function of concentration of DA and EP with linear trend line (b).

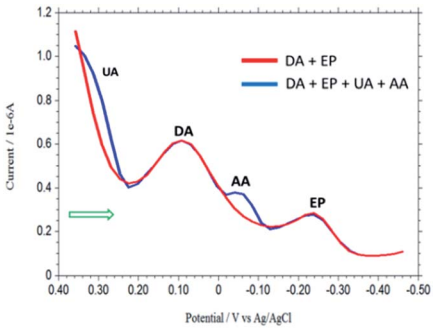

Fig. 4 DPVs of 0.2 μM DA and 0.2 μM EP and in presence of 1000 times higher concentration of AA and UA.

Effect of scan rate and kinetic analysis for DA and EP oxidation

The impacts of scan rate on the electrocatalytic oxidation of DA and EP at AgNPs–PCA–Au electrode were explored using cyclic voltammetry (Fig. S19 and S20†). The results showed that with increasing scan rate, the oxidation peak potential (E_{pa}) for DA and EP are shifted to more positive potential, confirming the kinetic limitation of the electrochemical reaction.[20] The anodic peak current (I_{pa}) *versus* the square root of the scan rate ($\sqrt{\nu}$) for DA and EP in the range of 20–100 mV s^{-1} was found to be linear following the linear regression equation I_{pa} (μA) = 0.7179ν (mV s^{-1}) + 0.9049 ($R^2 = 0.9944$) and I_{pa} (μA) = 0.1251ν (mV s^{-1}) + 0.6292 ($R^2 = 0.9954$), respectively. These observations revealed that the electrooxidation reaction of DA and EP was followed pure diffusion controlled electron transfer at AgNPs–PCA–Au electrode.[21] Using the plot (I_{pa} *versus* $\sqrt{\nu}$) and Randles–Sevcik equation[21]

$$I_{pa} = 2.69 \times 10^5 n^{3/2} A D^{1/2} C \nu^{1/2} \quad (1)$$

the diffusion coefficient (D) was calculated for DA and EP and the values obtained were 13.4 × 10^{-6} cm^2 s^{-1} and 2.1 × 10^{-6} cm^2 s^{-1}, respectively (where I_{pa} is the peak current, n is the number of electron transfer, $n = 2$ for DA and EP oxidation, A is the electrode area, C is the concentration of electroactive species, and ν is the scan rate at 298 K). The electron transfer coefficient for the quasireversible oxidation of DA and irreversible oxidation of EP at the modified electrode can be determined from the equation[21]

$$E_p - E_{p/2} = 1.857RT/\alpha F = 47.7/\alpha \text{ (mV)} \quad (2)$$

where E_p and $E_{p/2}$ represent the peak potential and the half-height peak potential, respectively in cyclic voltammetry experiment where R, F and T have their usual meaning. For DA and EP oxidation, ($E_p - E_{p/2}$) were 46 mV and 48 mV, respectively, hence electron transfer coefficient (α) is calculated to be 0.54 for DA and 0.49 for EP. The standard heterogeneous rate constant (k_s) for the oxidation of DA and EP at AgNPs modified gold electrode was calculated by using the Velasco equation[22]

$$k_s = 1.11 D^{1/2} (E_p - E_{p/2})^{-1/2} \nu^{1/2} \quad (3)$$

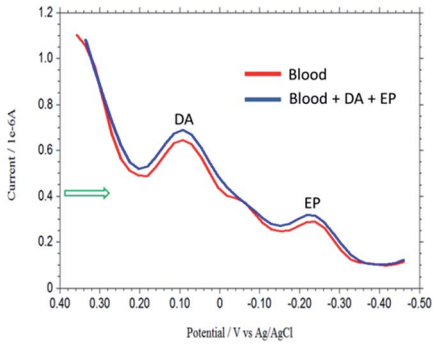

Fig. 5 Overlaid DPV of human blood sample solution and after addition of standard DA and EP.

The estimated k_s values for the oxidation of DA and EP at AgNPs–PCA–Au electrodes was found to be 6.1×10^{-3} cm s^{-1} and 2.4×10^{-3} cm s^{-1}, respectively. The observed higher k_s value for DA and EP at the modified electrode indicates that both the oxidation were faster at the AgNPs–PCA–Au electrode.

Effect of solution pH

The role of pH on the electrooxidation of DA and EP at AgNPs modified Au electrode were scrutinized in the pH range of 5.0–9.0 (Fig. S21a and S22a†). Exploration of the impact of pH on the peak current of DA and EP at the AgNPs–PCA–Au electrode tells that the peak current was reached maximum for DA and EP at pH 7.0 and thereafter decreased by increasing pH of the solution (Fig. S21b and S22b†). At pH 7.0, DA and EP mostly exists as a protonated form ($^{+}NH_3$-DOH or $^{+}NH_2$-EOH with D and E for DA and EP skeletons, respectively)[23,24] and therefore readily preconcentrated on the negatively charged [AgNPs–($^{-}$OOC–$C(NH_2)$–$C(CH_3)_2$–S)] thin layer modified gold electrode and showing maximum current height. Above pH 7.0, the anodic peak current decreased and this may be due to the repulsion between the anionic form of DA or EP (NH_2-DO^{-} or NH-EO^{-}) and the negatively charged AgNPs–($^{-}$OOC–$C(NH_2)$–$C(CH_3)_2$–S–Au electrode. By considering the pH dependency results, we have selected pH 7.0 for DA and EP in the subsequent experiments. The anodic peak potential for DA and EP changes linearly with pH between 5–9, and is shifted to more negative potentials following the linear regression equation E_{pa} (V) = −0.0604pH + 0.0629 (R^2 = 0.999) and E_{pa} (V) = −0.0596pH + 0.4406 (R^2 = 0.998), respectively (Fig. S21c and S22c†). The slope of 60.0 and 59.6 mV pH^{-1} suggested that equal number of protons and electrons were participated in the electrode reaction process.[25] The negative shifting of anodic peak potential indicates that the proton liberation from DA and EP is facilitated (less energy required for DA and EP oxidation) with increasing pH of the medium.

Reproducibility, sensitivity and stability

Reproducibility and long term stability is highly desirable for the practical applications and commercialization of any electrochemical sensor. The reproducibility of the AgNPs–PCA–Au electrode was examined by 10 repetitive measurements for DA and EP in 0.1 M PBS solution. The results showed that the oxidative peak current for DA and EP remain same with a relative standard deviation (RSD) of 0.04 and 0.03%, respectively, suggesting that the modified electrode has a good reproducibility. The AgNPs modified gold electrode was highly sensitive towards DA and EP and the sensitivity were 97.33 and 52.3 μA cm^{-2} μM^{-1}, respectively. The long term stability was monitored by taking CV at 5 days intervals for 30 days. After each use the sensor was washed, dried and stored at room temperature by covering with a rubber cap. Up to 30 days monitoring, the sensor retained 100% of its original current response for DA and EP in 0.1 M PBS.

Interference study

The influence of various interfering agents such as ascorbic acid, uric acid, citric acid, cysteine, glucose and different ions *e.g.* Na^{+}, K^{+}, Cl^{-} *etc.* on the determination of DA and EP were evaluated under optimum conditions. Fig. S23 and S24† shows the amperometric response for DA and EP at AgNPs–PCA–Au electrode in the presence of tenfold excess interferents at 0.22 and 0.18 V, respectively in 0.1 M PBS under stirring condition. With the addition of these interfering substances no obvious current response was observed, however, with the addition of DA and EP the sharp current response were appeared. These results suggest that the sensor is highly selective for DA and EP detection.

Real sample analysis

To evaluate the feasibility of proposed AgNPs–PCA–Au sensor for the determination of DA and EP in real sample, human whole blood was taken. Standard addition method was used to determine the ability of the proposed electrochemical sensor. Fig. 5 shows the DPV of blood sample solution (1.0 mL blood samples diluted with 4 mL 0.1 M in PBS, pH 7.0) and after addition of standard DA and EP solution in blood sample solution. The DPV of blood sample shows the reduction of DA and EP at 0.09 V and 0.23 V, respectively. The content of DA and

Table 1 Determination of DA, EP, AA and UA in blood sample

Analyte in blood	Detected (μM)	Spiked (μM)	Found (μM)	RSD[a] (%)	Recovery (%)
DA	0.42	0.2	0.201	1.14	100.5
EP	0.21	0.2	0.198	1.21	99.0
AA	62.14	10.0	10.030	2.37	100.3
UA	36.27	15.0	15.240	1.53	101.6

[a] Five times measurement were taken.

EP in blood sample was calculated 0.42 μM (0.0064 mg dL^{-1}) and 0.21 μM (0.0039 mg dL^{-1}), respectively using the standard addition method and the direct interpolation of the linear regression (RSD = 1.14% and RSD = 1.21% for DA and EP, respectively). The accuracy of the method was also verified by recovery study by adding standard DA and EP solution to the real sample and around 99–100.5% recoveries were obtained. The same sensor can able to detect AA and UA in blood sample (Fig. S25†). The results are summarized in Table 1. The results indicate that the modified electrode can effectively detect DA, EP, UA and AA in human blood sample.

Conclusions

In this communication, a new electrochemical sensor AgNPs–penicillamine–Au was introduced for the simultaneous determination of DA and EP in presence of AA and UA. DPV shows all four distinct reduction peaks for DA, EP, AA and UA. The sensor showed high sensitivity, excellent selectivity, and long linear dynamic range with low detection limit of as low as nanomolar range. Furthermore, the sensor has higher potential for real sample application and was proved by the simultaneous determination of DA, EP and AA, UA in human blood sample.

References

1 D. J. Michael and R. M. Wightman, *J. Pharm. Biomed. Anal.*, 1999, **19**, 33; R. M. Wightman, L. J. May and A. C. Michael, *Anal. Chem.*, 1988, **60**, 769A.

2 J. W. Zheng, Y. Yang, S. H. Tian, J. Chen, F. A. W. Wilson and Y. Y. Ma, *Neurosci. Lett.*, 2005, **382**, 164; N. Nakao and T. Itakura, *Prog. Neurobiol.*, 2000, **61**, 313.

3 T. N. Deftereos, A. C. Calokerinos and C. E. Efstathiou, *Analyst*, 1993, **118**, 627; M. H. Sorouraddin, J. L. Manzoori, E. Kargarzadeh and A. M. Haji Shabani, *J. Pharm. Biomed. Anal.*, 1998, **18**, 877.

4 V. Carrera, E. Sabater, E. Vilanova and M. A. Sogorb, *J. Chromatogr., B: Anal. Technol. Biomed. Life Sci.*, 2007, **847**, 88.

5 J. Z. Kang, X. B. Yin, X. R. Yang and E. K. Wang, *Electrophoresis*, 2005, **26**, 1732.

6 Y. Y. Su, J. Wang and G. N. Chen, *Talanta*, 2005, **65**, 531.

7 N. T. Deftereos, A. C. Calokerinos and C. E. Efstlectrochathiou, *Analyst*, 1993, **118**, 627; J. X. Du, L. H. Shen and J. R. Lu, *Anal. Chim. Acta*, 2003, **489**, 183–189.

8 M. Zhu, X. Huang, J. Li and S. Hansi, *Anal. Chim. Acta*, 1997, **357**, 261.

9 Y. Wang and Z.-Z. Chen, *Colloids Surf., B*, 2009, **74**, 322.

10 Y. Zhang, W. Ren and S. Zhang, *Int. J. Electrochem. Sci.*, 2013, **8**, 6839.

11 A. Ulman, *Chem. Rev.*, 1996, **96**, 1533.

12 Q. Wang, D. Dong and N. Li, *Bioelectrochemistry*, 2001, **54**, 169.

13 L. M. Niu, H. Q. Luo and N. B. Li, *Microchim. Acta*, 2005, **150**, 87–93.

14 Y. G. Sun and Y. N. Xia, *Science*, 2002, **298**, 2176.

15 T. Sun and K. Seff, *Chem. Rev.*, 1994, **94**, 857.

16 F. J. Smally, K. Chalfant, S. W. Feldberg, T. M. Nahir and E. F. Bowden, *J. Phys. Chem. B*, 1999, **103**, 1676.

17 R. K. Shervedani, A. Hatefi-Mehrjardi and M. Khosravi Babadi, *Electrochim. Acta*, 2007, **52**, 7051.

18 T. A. Afify, H. H. Saleh and Z. I. Ali, *Polym. Compos.*, 2015, DOI: 10.1002/pc23866; B. Ajitha, Y. A. K. Reddy and P. S. Reddy, *Powder Technol.*, 2015, **269**, 110.

19 P. N. Mashazi, P. Westbroek, K. I. Ozoemena and T. Nyokong, *Electrochim. Acta*, 2007, **53**, 1858.

20 C. S. Shen, Y. Z. Wen, Z. L. Shen, J. Wu and W. P. Liu, *J. Hazard. Mater.*, 2011, **193**, 209.

21 A. J. Bard and L. R. Faulkner, *Electrochemical Methods Fundamental and Applications*, John Wiley & Sons Inc., New York, 2001.

22 J. G. Velasco, *Electroanalysis*, 1997, **9**, 880.

23 J. L. Berfield, L. C. Wang and M. E. A. Reith, *J. Biol. Chem.*, 1999, **274**, 4876.

24 R. C. Reynolds and H. F. Hardman, *Eur. J. Pharmacol.*, 1972, **20**, 249.

25 E. Laviron, *J. Electroanal. Chem.*, 1974, **52**, 355.

Annexure

List of Publications

(Publications Nos. 1, 2, 3 & 4 included in the Thesis)

1. Electrocatalytic oxidation of ascorbic acid by immobilized silver nanoparticles on self-assembled L-cysteine monolayer modified gold electrode. **K. Barman** and Sk. Jasimuddin, *Indian J. Chem., Sect. A.*, 2014, **53A**, 57.
2. Electrochemical detection of adenine and guanine using a self-assembled copper(II)– thiophenyl-azoimidazole complex monolayer modified gold electrode. **K. Barman** and Sk. Jasimuddin, *RSC Adv*., 2014, **4**, 49819.
3. Non-enzymatic electrochemical sensing of glucose and hydrogen peroxide using a bis(acetylacetonato)oxovanadium(IV) complex modified gold electrode. **K. Barman** and Sk. Jasimuddin, *RSC Adv*., 2016, **6**, 20800.
4. Simultaneous electrochemical detection of dopamine and epinephrine in the presence of ascorbic acid and uric acid using a AgNPs–penicillamine–Au electrode. **K. Barman** and Sk. Jasimuddin, *RSC Adv*., 2016, **6**, 99983.
5. Electrocatalytic oxidation of hydroquinone with Cu^{2+} modified gold-L-cysteine self-assembled monolayer electrodes. **K. Barman** and Sk. Jasimuddin, *Indian J. Chem., Sect. A.*, 2013, **52A**, 217-220.
6. Bifunctional gold–manganese oxide nanocomposites: benign electrocatalysts toward water oxidation and oxygen reduction. H. Rahaman, **K. Barman**, Sk. Jasimuddin and S. K. Ghosh, *RSC Adv.*, 2014, **4**, 41976.
7. Fluid interface-mediated nanoparticle membrane as an electrochemical sensor. M. Ali, **K. Barman**, Sk. Jasimuddin and S. K. Ghosh, *RSC Adv.*, 2014, **4**, 41976.
8. Electrocatalytic oxidation of water by a selfassembled oxovanadiumIJIV) complex modified gold electrode. **K. Barman** and Sk. Jasimuddin, *Catal. Sci. Technol.*, 2015, **5**, 5100.
9. Cerium(III) Complex Modified Gold Electrode: An Efficient Electrocatalyst for the Oxygen Evolution Reaction. S. Garain, **K. Barman**, T. K. Sinha, Sk. Jasimuddin, J.

Haeberle, K. Henkel, D. Schmeisser, and D. Mandal, *ACS Appl. Mater. Interfaces*, 2016, **8**, 21294.

10. Hybrid Mn_3O_4–NiO nanocomposites as efficient photoelectrocatalysts towards water splitting under neutral pH conditions. H. Rahaman, **K. Barman**, Sk. Jasimuddin and S. K. Ghosh, *RSC Adv.*, 2016, **6**, 113694.
11. MnO doped SnO_2 nanocatalysts: Activation of wide band gap semiconducting nanomaterials towards visible light induced photoelectrocatalytic water oxidation. D. Mohanta, **K. Barman**, Sk. Jasimuddin and Md. Ahmaruzzaman, *Journal of Colloid and Interface Science*, 2017, **505**, 756.

List of Seminar/Conference /Symposium/Workshops Attended

1. Presentation of paper entitled "Electrocatalytic water oxidation using carbon nanomaterial at pH 7" in the 'International conference on Material Science-2017' organized by the Department of Physics, Tripura University, Tripura from 16-18 February, 2017.
2. Presentation of paper entitled "Electrochemical water oxidation using phosphomolybdic acid nanoparticles modified gold electrode" in the 'National Symposium on Advances in Chemical Sciences-2017' in the Department of Chemistry, Assam University, Silchar from 11-12 January, 2017.
3. Presentation of paper entitled "Electrochemical sensing and catalytic activity of vanadium complex modified gold electrode towards glucose and hydrogen peroxide" in the national conference, 'MRSI North-East Symposium on Advanced Materials for Sustainable Application' conducted by CSIR-North East Institute of Science and Technology, Jorhat from 18-21st February, 2016.
4. Presentation of paper entitled "Electrocatalytic oxidation of water using vanadium complex modified gold electrode" in the national conference on 'Current Perspectives on Research on Chemical Sciences' in Department of Chemistry, Assam University, Silchar on 25 - 26th March, 2015.
5. Presentation of paper entitled "Electrocatalytic oxidation of ascorbic acid by immobilized silver nanoparticles on self-assembled L-cysteine monolayer modified gold electrode" in the 'National Seminar on Advances in Biotechnology Research: Current Trends and Future Prospects, 2014' in Department of Biotechnology, Assam University, Silchar on 25 - 26th March, 2014.